AMP-activated protein kinase and adenylate kinase prevent the ATP catastrophe and cytotoxic protein aggregation

Masak Takaine[1,2]*, Hiromi Imamura[3], Satoshi Yoshida[1,2,4,5]*

[1]Gunma University Initiative for Advanced Research (GIAR), Gunma University, Maebashi 371-8512, Japan
[2]Institute for Molecular and Cellular Regulation (IMCR), Gunma University, Maebashi 371-8512, Japan
[3]Graduate School of Biostudies, Kyoto University, Kyoto 606-8501, Japan
[4]School of International Liberal Studies, Waseda University, Tokyo, 169-8050, Japan
[5]Japan Science and Technology Agency, PREST

*Correspondence should be addressed to: masaktakaine@gunma-u.ac.jp (M.T.) (Lead contact) or satosh@waseda.jp (S.Y.)

Running title

ATP homeostasis prevents cytotoxic protein aggregation

Keywords

ATP, homeostasis, proteostasis, yeast, neurodegenerative disease, AMPK, protein aggregation

ABSTRACT

ATP is the main source of chemical energy in all life and is maintained at several millimolar in eukaryotic cells. However, the mechanisms responsible for and physiological relevance of this high and stable concentration of ATP remain unclear. We herein demonstrate that AMP-activated protein kinase (AMPK) and adenylate kinase (ADK) cooperate to maintain cellular ATP levels regardless of glucose concentrations. Single cell imaging of ATP-reduced yeast mutants revealed that ATP concentrations in these mutants underwent stochastic and transient depletion of ATP repeatedly, which induced the cytotoxic aggregation of endogenous proteins and pathogenic proteins, such as huntingtin and α-synuclein. Moreover, pharmacological elevations in ATP levels in an ATP-reduced mutant prevented the accumulation of α-synuclein aggregates and its cytotoxicity. The removal of cytotoxic aggregates depended on proteasomes, and proteasomal activity cooperated with AMPK or ADK to resist proteotoxic stresses. The present results provide the first evidence to show that cellular ATP homeostasis ensures proteostasis and revealed that stochastic fluctuations in cellular ATP concentrations contribute to cytotoxic protein aggregation, implying that AMPK and ADK are important factors that prevent proteinopathies, such as neurodegenerative diseases.

INTRODUCTION

Adenosine triphosphate (ATP) is the main energy currency used by all living organisms. Due to high demand, the turnover rate of ATP is estimated to be less than one minute in yeast and metazoans (Mortensen, Thaning et al., 2011, Takaine, Ueno et al., 2019). In addition to its role as energy currency, recent studies reported that ATP may influence the balance between the soluble and aggregated states of proteins, suggesting that proteostasis is maintained by energy-dependent chaperones and also by the property of ATP as a hydrotrope to solubilize proteins (Hayes, Peuchen et al., 2018, Patel, Malinovska et al., 2017). Recent proteomic analyses demonstrated that many cellular proteins are insoluble at submillimolar ATP concentrations and become soluble at ATP concentrations > 2 mM (Sridharan, Kurzawa et al., 2019); however, it currently remains unclear whether ATP-dependent protein solubilization/desolubilization play any significant roles in cell physiology.

We recently established a reliable imaging technique to quantify intracellular ATP concentrations in single living yeast cells using the genetically encoded fluorescent ATP biosensor QUEEN (Yaginuma, Kawai et al., 2014), which enables long-term evaluations of ATP homeostasis in individual cells (Takaine et al., 2019). Our findings demonstrated that intracellular ATP concentrations did not vary within a yeast population grown in the same culture (Takaine et al., 2019), which was in contrast to the large variations observed in intracellular ATP concentrations within a bacterial cell population (Yaginuma et al., 2014). Moreover, intracellular ATP concentrations in individual living yeast cells were stably and robustly maintained at approximately 4 mM, irrespective of carbon sources and cell cycle stages, and temporal fluctuations in intracellular ATP concentrations were small (Takaine et al., 2019). Based on these findings, we hypothesized that an exceptionally robust mechanism may exist to precisely regulate ATP concentrations in eukaryotes. It also remains unclear why ATP is stably maintained at a markedly higher concentration than the K_m (Michaelis constant) required for the enzymatic activity of almost all ATPases (Edelman, Blumenthal et al., 1987), and the consequences associated with failed ATP homeostasis in living organisms have not yet been elucidated.

The most promising candidate regulator of ATP homeostasis is AMP-activated protein kinase (AMPK). AMPK, which is activated by AMP and inhibited by ATP (Xiao, Heath et al., 2007), has long been regarded as an important regulator of the whole-body and cellular energy status in eukaryotes (Hardie, Schaffer et al., 2016). AMPK is activated by increases in the AMP:ATP or ADP:ATP ratio (*i.e.,* low-energy state), and regulates its downstream effectors

by phosphorylation to redirect cell metabolism from an anabolic (ATP-consuming) state to catabolic (ATP-producing) state (Herzig & Shaw, 2017). In the budding yeast *Saccharomyces cerevisiae*, the sucrose non-fermenting 1 (Snf1) protein kinase complex is the sole AMPK. Similar to other AMPKs, the yeast Snf1 complex comprises three subunits: the catalytic α subunit (*SNF1*), scaffolding β subunit (*SIP1*, *SIP2* or *GAL83*), and regulatory γ subunit (*SNF4*) (Ghillebert, Swinnen et al., 2011). The role of the Snf1 complex in adaptation to glucose limitations has been characterized in detail (Hedbacker & Carlson, 2008). In the presence of sufficient glucose in the medium, the Snf1 complex is inactive (Wilson, Hawley et al., 1996). When glucose concentrations decrease, the Snf1 complex is activated and phosphorylates the transcriptional repressor Mig1, which then triggers the transcription of numerous glucose-repressed genes (Carlson, 1999). However, the contribution of AMPK or the Snf1 complex to cellular ATP levels remains unknown.

Other possible candidate regulators of ATP homeostasis include genes whose mutation leads to decreases in the cellular content of ATP. However, based on biochemical analyses of cell populations, few yeast mutants reduced ATP levels (Gauthier, Coulpier et al., 2008, Ljungdahl & Daignan-Fornier, 2012). Adenylate kinase (ADK) is a key enzyme that synthesizes ATP and AMP using two ADP molecules as substrates, and the null-mutant of ADK (*adk1*Δ) was shown to have a reduced cellular ATP concentration (~70% of the wild type) (Gauthier et al., 2008). Bas1 is a transcription factor that is required for *de novo* purine synthesis and *bas1*Δ has also a reduced ATP concentration (~50% of the wild type) (Gauthier et al., 2008). However, the regulation of ATP concentrations and the physiological consequences of reduced ATP levels in these mutants remain unclear, particularly at the single cell level.

In the present study, we investigated the roles of AMPK, ADK, and Bas1 in ATP homeostasis using the QUEEN-based single cell ATP imaging technique. We demonstrated for the first time that AMPK is involved in the regulation of intracellular ATP concentrations, even under glucose-rich conditions. Furthermore, time-lapse ATP imaging revealed that cells lacking both AMPK and ADK frequently underwent transient ATP depletion, while ATP concentrations oscillated in those lacking Bas1. These ATP dynamics in the mutants were overlooked in previous biochemical studies. We found that some intrinsic proteins and aggregation-prone model proteins, including α-synuclein, which is responsible for Parkinson's disease, aggregated and were cytotoxic in all of the ATP-reduced mutants tested. The present results suggest that the stable maintenance of ATP is essential for proteostasis and imply that

111 an ATP crisis promotes proteinopathies, such as neurodegenerative diseases.

RESULTS

AMPK is involved in the maintenance of cellular ATP levels

We recently developed a reliable monitoring system for cytoplasmic ATP concentrations in living yeast cells using the ATP biosensor QUEEN (Takaine et al., 2019). We conducted a more detailed examination of ATP dynamics in wild-type and mutant yeast cells using this system in the present study. We investigated whether the deletion of *SNF1*, which encodes a catalytic subunit of AMPK, affects cellular ATP concentrations. In *SNF1*-null mutant (*snf1*Δ) cells, cellular ATP levels were significantly lower than those in wild-type cells at all glucose concentrations tested (2, 0.2, and 0.05%) (Fig. 1A, B). It is important to note that even under high glucose conditions (2% glucose), in which the Snf1 complex is considered to be inactive, *snf1*Δ cells showed significantly reduced ATP levels. Moreover, the deletion of each gene encoding the β subunit of AMPK (*SIP1*, *SIP2*, or *GAL83*) reduced cellular ATP levels to a similar extent as the deletion of *SNF1*, suggesting that three subtypes of the Snf1 complex are involved in maintaining ATP concentrations (Fig. 1C). On the other hand, the deletion of *MIG1*, which encodes a major downstream target of the Snf1 complex in glucose repression, had a negligible effect on ATP levels (Fig. 1D), suggesting that unknown factors other than Mig1 primarily regulate ATP levels under the control of the Snf1 complex. Collectively, these results demonstrated for the first time that AMPK/SNF1 affect cellular ATP concentrations even under glucose-rich conditions.

Adenylate kinase ADK1 cooperates with AMPK to regulate ATP homeostasis

Adenylate kinase catalyzes the interconversion of adenine nucleotides (ATP+AMP ⟷ 2ADP), which is important for *de novo* adenine nucleotide synthesis and the balance of ATP, ADP, and AMP. Previous biochemical studies reported that the deletion of the adenylate kinase gene reduced ATP concentrations in mouse skeletal muscle cells and budding yeasts (Gauthier et al., 2008, Janssen, Dzeja et al., 2000). We confirmed these findings using an ATP imaging method: *adk1*Δ cells showed significantly lower QUEEN ratios than wild-type cells on average in the presence of sufficient carbon sources (Fig. S1).

In addition to being a key enzyme in purine metabolism, adenylate kinase has also been suggested to cooperate with AMPK in order to monitor the cellular energy state (Hardie, Carling et al., 1998). Therefore, we compared ATP levels in *snf1*Δ *adk1*Δ double mutant cells with those in *snf1*Δ, *adk1*Δ, and wild-type cells (Fig. 2A, B). The data obtained were represented by a dot plot that shows distribution characteristics in extensive detail. *snf1Δ adk1Δ* cells had significantly lower average ATP levels than single mutant cells. We also

found not only a general reduction, but also a huge variation in ATP levels in the *snf1*Δ, *adk1Δ, snf1*Δ *adk1Δ* cell population, as indicated by the large coefficient of variance (CV) (Fig. 2B). Furthermore, some cells had extremely low ATP levels in *snf1Δ adk1Δ* (Fig. 2A, B). These results suggest that Adk1 and the Snf1 complex both synergistically contribute to ATP homeostasis.

A large pool of adenine nucleotide is important for maintaining cellular ATP concentrations

We also examined a *bas1Δ* mutant, which is defective in the expression of genes responsible for adenine biogenesis (Daignan-Fornier & Fink, 1992, Denis, Boucherie et al., 1998). Consistent with previous biochemical findings (Gauthier et al., 2008), ATP levels quantified by QUEEN were reduced by ~50% in *bas1Δ* cells (Fig. 2C, D). We found not only a general reduction, but also a large variation in ATP levels in the *bas1Δ* cell population, as indicated by the large CV (Fig. 2D). The decrease observed in ATP levels was due to reduced adenine biosynthesis because the addition of extra adenine to media partially restored ATP levels (Fig. 2D). These results suggest that the sufficient production of adenine nucleotides is essential for the stable maintenance of ATP levels. Moreover, the role of Bas1 in maintaining ATP levels appeared to be epistatic to that of Snf1 because *bas1Δ snf1Δ* double mutant cells showed a similar distribution of ATP levels to *bas1Δ* cells (Fig. S2).

ATP levels temporally fluctuate in ATP mutant cells

To investigate the mechanisms contributing to the large variations in ATP concentrations in *snf1Δ adk1Δ* cells in more detail, we employed time-lapse ATP imaging (Fig. 3). We found that the QUEEN ratio often underwent a rapid decline followed by recovery in *snf1Δ adk1Δ* cells (see 116 and 132 min in Fig. 3A, C, and Movie S1, and 180 and 356 min in Fig. 3B, D, and Movie S2). The sudden decrease in ATP concentrations (hereafter called “the ATP catastrophe”) occurred within a few minutes without any sign and was rarely observed in wild-type cells (Takaine et al., 2019). The ATP catastrophe appeared to be a stochastic event and cell intrinsic: these events occurred independent of cell cycle stages or cell sizes (compare Fig. 3C with D). Under some conditions, the QUEEN ratio did not recover after the ATP catastrophe and the cell died, as judged by the loss of QUEEN signals in the cell (Fig. S3). These results suggest that the large variations in ATP concentrations observed in *snf1Δ adk1Δ* cells were not simply due to a mixed population with different basal ATP levels, but were rather due to the stochastic ATP catastrophe in individual cells.

Time-lapse imaging of *bas1Δ* revealed oscillatory cycles in ATP concentrations (Figs. 3E and S4A, and Movies S3 and S4): ATP cycling in *bas1Δ* cells was slow (~35 min on average, Fig. S4B) and distinguishable from that in *snf1Δ adk1Δ* cells; however, the common characteristics of these mutants were that the concentration of ATP repeatedly reached close to 0 mM. The ATP oscillation cycle was unsynchronized in the population and independent of cell cycle progression, suggesting a unique metabolic rhythm intrinsic to each cell. The oscillatory nature of ATP cycling in the *bas1Δ* mutant may involve a transcription/translation cycle and will be described elsewhere.

ATP homeostasis is required for preventing protein aggregation.

We recently reported that cellular ATP concentrations are stably maintained at ~4 mM in budding yeast (Takaine et al., 2019) and herein demonstrated that in the Snf1/AMPK complex, Adk1 and Bas1 are required for the regulation of ATP homeostasis. However, the physiological importance of ATP homeostasis remains unknown. To clarify the significance of high ATP concentrations, we examined the global genetic interactions of *snf1Δ*, *adk1Δ*, and *bas1Δ* using CellMap ((Usaj, Tan et al., 2017), thecellmap.org). An *in silico* analysis identified genes involved in "protein folding/glycosylation" as common negative genetic interactors with *adk1Δ* and *bas1Δ* (Fig. 4A). Negative genetic interactors of *ura6*, a gene encoding uridylate kinase that also exhibits adenylate kinase activity, were enriched in the "protein folding/glycosylation" category (Fig. 4A). We also found that interactors of *snf1* were implicated in "protein folding/glycosylation. None of these mutants exhibited apparent genetic interactions with genes in the "metabolism" category (Fig. 4A). The same analysis using genetic and physical interactors provided similar results and showed that many interactors were enriched in the "protein turnover" category (Fig. S5). These results imply that although these three mutants regulate ATP with distinct mechanisms, all three have a common cellular function.

To examine possible defects in protein folding and turnover (*i.e.*, proteostasis), we challenged these mutants with various proteotoxic stresses. We found negligible growth defects in ATP mutants under normal growth conditions with 2% glucose at 30°C (control in Fig. 4B), suggesting that a high concentration of ATP is not necessary for cellular growth. However, the *adk1* and *bas1* mutants both exhibited severe growth defects with a high temperature of 40°C, 1 hour of heat shock at 55°C, or in the presence of 0.5 μg/ml of the glycosylation inhibitor tunicamycin or 2 mM H_2O_2. The *SNF1* deletion increased the stress sensitivity of *adk1Δ* (Fig. 4B). This sensitivity to proteotoxic stress suggests that ATP homeostasis mutants

are defective in some aspects of proteostasis. We found that all four mutants tested contained significantly increased numbers of Hsp104-GFP foci, a marker of protein aggregation (Josefson, Andersson et al., 2017) (Fig. 4C, D). In contrast to Hsp104-GFP foci, Pab1-GFP, a marker of stress granule (SG) assembly (Hoyle, Castelli et al., 2007), did not form foci in ATP mutants, suggesting that protein aggregation and SG assembly are regulated in a distinct manner (Fig. 4D). These analyses identified abnormal protein aggregation as a common defect associated with ATP homeostasis mutants for the first time.

The transient depletion of ATP leads to the formation of protein aggregates

To examine whether ATP depletion triggers protein aggregation in living yeast, we artificially depleted cellular ATP levels by replacing glucose with 2-deoxyglucose (2DG), a strong inhibitor of glycolysis, in the media and monitored protein aggregation using Hsp104-GFP as a marker of protein aggregation (Josefson et al., 2017) in wild-type cells. We previously showed that ATP levels were almost completely depleted 2 minutes after the 2DG treatment (Takaine et al., 2019). Within 15 min of the 2DG treatment, more than 20% cells contained Hsp104-GFP foci indicative of protein aggregation (Fig. 5A, B). In contrast to ATP, the concentration of which recovers to normal levels within 1 min of glucose refeeding (Takaine et al., 2019), the dissolution kinetics of Hsp104-GFP were significantly slower (up to hours, Fig. 5A, B).

To further confirm whether a high concentration of ATP is required for protein solubility, we also tested the Ubc9-ts protein, a model protein that is prone to aggregate (Kaganovich, Kopito et al., 2008), and found that ATP depletion by the 2DG treatment triggered Ubc9-ts protein aggregation (Fig. 5C). Thus, not only Hsp104-GFP-positive intrinsic proteins, but also extrinsic model proteins aggregate after ATP depletion.

SG are assembled in budding yeast cells after stressful conditions, such as glucose depletion (Hoyle et al., 2007). In contrast to the formation of Hsp104-GFP foci, ATP depletion after the 2DG treatment did not instantly trigger the formation of SG (Fig. S6). Consistent with recent findings (Jain, Wheeler et al., 2016), the present results suggest that SG formation requires ATP. We also noted that Hsp104-GFP foci and SG did not co-localize, suggesting that these structures are derived from distinct mechanisms (Fig. S6). Thus, the artificial depletion of ATP may trigger abnormal protein aggregation in living yeast cells.

ATP homeostasis is required for the protection of cells from cytotoxicity caused by protein aggregation

Protein aggregation is often associated with neurodegenerative diseases, such as Alzheimer's, Huntington's, and Parkinson's diseases (Eftekharzadeh, Hyman et al., 2016). Mitochondrial failure has also been associated with many neurodegenerative diseases; however, it currently remains unclear whether energy failure causes protein aggregation because mitochondria also produce cytotoxic reactive oxygen species (ROS). (Bhat, Dar et al., 2015, Pathak, Berthet et al., 2013). The abnormal aggregation of α-synuclein has been implicated in Parkinson's disease (Lashuel, Overk et al., 2013). To clarify whether ATP is preventing the formation of cytotoxic protein aggregation, we examined the toxicity of α-synuclein-GFP (Syn-GFP) in budding yeast. As reported previously, the expression of Syn-GFP exhibited negligible toxicity against wild-type yeast when expressed under the inducible *GAL1* promotor (Fig. 6A) (Outeiro & Lindquist, 2003, Sharma, Brandis et al., 2006, Wijayanti, Watanabe et al., 2015). However, *snf1Δ*, *adk1Δ*, and *bas1Δ* are hypersensitive to the expression of Syn-GFP (Fig. 6A). We also found that *rpn4Δ*, which encodes a key transcription factor for proteasomal subunits (Xie & Varshavsky, 2001), was very sensitive to Syn-GFP (Fig. 6A), which is consistent with the concept that Syn-GFP is degraded in the ubiquitin-proteasomal pathway in yeast (Tofaris, Kim et al., 2011, Wijayanti et al., 2015). We then visualized the cellular localization of Syn-GFP. Consistent with previous findings (Willingham, Outeiro et al., 2003), Syn-GFP expressed in yeast mainly localized to the plasma membrane (Fig. 6B, C). In addition to the plasma membrane, we found that Syn-GFP localized to punctated structures, most likely corresponding to protein aggregation (Fig. 6B, C). Punctated structures were not as obvious in *rpn4Δ* cells defective in proteasomes, suggesting that the accumulation of Syn-GFP puncta was not simply due to defective degradation.

To investigate whether a high concentration of ATP protects cells from toxic protein aggregation, we added extra adenine to the medium (Fig. 6D). A previous study demonstrated that the addition of 300 μM adenine to the medium increased ATP concentrations from 4 to 5.5 mM in wild-type cells and from 1 to 4 mM in *bas1Δ* cells (Gauthier et al., 2008) (similar results are shown in Fig. 2D), but induced little or no changes in *adk1Δ* cells (from 2 to 2 mM) (Gauthier et al., 2008). Consistent with our hypothesis, the addition of adenine reduced Syn-GFP toxicity and aggregation in *bas1Δ*, but not *adk1Δ* cells (Fig. 6D). Thus, a high concentration of ATP prevented Syn-GFP aggregation and toxicity.

We examined another model protein involved in neurodegenerative diseases. PolyQ

containing the huntingtin protein tends to aggregate and has been implicated in Huntington's disease (Jiang, Poirier et al., 2005). We investigated the toxicity of Htt103Q, a mutant form of the huntingtin protein, which tends to aggregate and cause cytotoxicity in yeast (Meriin, Zhang et al., 2002). Consistent with the concept that a high concentration of ATP prevents protein aggregation, the ATP homeostasis mutants *snf1Δ*, *adk1Δ*, *snf1Δ adk1Δ*, and *bas1Δ* were very sensitive to Htt103Q expression (Fig. S7).

Proteasomes are essential for the removal of protein aggregates caused by ATP depletion

Protein aggregation caused by ATP depletion was cytotoxic (Figs. 4B and 6A) and was not easily dissolved after ATP repletion (Fig. 5). To identify a pathway that is essential for the removal of aggregates, we examined the involvement of proteasomes and autophagy.

The deletion of *RPN4*, which encodes a transcription factor of proteasomal genes (Xie & Varshavsky, 2001), down-regulated proteasomal activity (Kruegel, Robison et al., 2011) and resulted in synthetic growth defects with *adk1Δ*, *snf1Δ bas1Δ* at a high temperature of 38°C and in the presence of H_2O_2 (Fig. 6E). In contrast to proteasomes, autophagy did not appear to have genetic interactions with the above mutants (Fig. 6E). The deletion of an essential component of the autophagic pathway, *ATG1* did not affect the sensitivity of *adk1Δ*, *snf1Δ*, *bas1Δ* to a high temperature of 38°C or to H_2O_2 (Fig. 6E). We also did not observe the accumulation of Hsp104-GFP foci in the autophagy mutants *atg1*, *atg8*, and *atg13* (not shown).

To investigate the involvement of proteasomes in the removal of protein aggregates after the transient depletion of ATP, we pretreated cells with the proteasomal inhibitor MG132 or DMSO and examined the kinetics for the formation of Hsp104-GFP foci after the 2DG treatment (Fig. 6F) using the drug-sensitive yeast strain Y13206 (Piotrowski, Li et al., 2017). Under both conditions, more than 90% of cells exhibited Hsp104-GFP foci within 30 min of the 2DG treatment. More than two-thirds of Hsp104-GFP foci dissolved in the DMSO control, while less than one-third dissolved in MG132-treated samples, indicating that proteasomes are required for the dissolution process (Fig. 6F).

DISCUSSION

In the present study, we demonstrated for the first time that the Snf1 complex, budding yeast AMPK, is required for the stable maintenance of cellular ATP concentrations (ATP homeostasis) in collaboration with the adenylate kinase Adk1 (Fig. 7A). This function of the Snf1 complex in ATP homeostasis is independent of glucose concentrations in the medium and Mig1, the major transcriptional repressor involved in glucose repression (Fig. 1); therefore, this is distinct from its well-characterized role in adaptation to glucose limitations. The activity of the Snf1 kinase complex may be sharply tuned depending on the intracellular concentrations of adenine nucleotides or other metabolites indicative of cellular energy to prevent a rapid ATP catastrophe (Fig. 3), even in the presence of sufficient amounts of glucose. It is important to note that the reductions observed in intracellular ATP concentrations in *snf1Δ* cells in the presence of glucose were overlooked in previous biochemical analyses, again demonstrating the usefulness of QUEEN-based ATP imaging.

Since the deletion of *BAS1* caused the greatest reduction in ATP levels and is epistatic to *snf1Δ*, a large pool size of adenine nucleotide is a prerequisite for ATP homeostasis. This assumption is reasonable because the pool size of recyclable ATP restricts ATP concentrations based on the rapid turnover rate of ATP. Bas1 maintains the pool size of ATP by balancing ATP synthesis and irreversible decreases, such as incorporation into RNA and DNA (following conversion to deoxy-ATP), degradation, and excretion in rapidly proliferating yeasts.

We also showed that key regulators of ATP homeostasis play roles in preventing cytotoxic protein aggregation in budding yeast (Fig. 7B). The common feature associated with these mutants is reduced ATP levels, suggesting that high ATP levels are essential for protein solubilization.

A recent study suggested that the requirement for ATP changes depending on its concentration. At concentrations lower than 0.5 mM, ATP mainly serves as a substrate for enzymes, such as protein kinases and heat shock protein chaperones, whereas at concentrations higher than 2 mM, ATP may exert solubilizing effects on disordered proteins (Sridharan et al., 2019). ATP homeostasis may also be required to constantly drive proteasomal protein degradation, which requires large amounts of ATP (Benaroudj, Zwickl et al., 2003, Tanaka, Waxman et al., 1983).

Previous biochemical measurements indicated that although ATP levels were lower in *adk1* and *bas1* mutants than in the wild type, these mutants still had ATP concentrations that were higher than 2 mM (Gauthier et al., 2008), which does not directly explain the accumulation of protein aggregates in these mutants (Fig. 4) because most proteins are expected to be soluble at > 2 mM ATP (Sridharan et al., 2019). The visualization of ATP dynamics in living cells at the single cell level revealed that ATP undergoes transient depletion repeatedly (the ATP catastrophe) in AMPK and ADK mutants, which explains how aggregation-prone proteins aggregate and cause cytotoxicity. A similar, but distinct instability of ATP was observed in *bas1Δ*, further confirming that the ATP catastrophe causes protein aggregation. Although severe ATP depletion in these mutants was gradually recovered by as yet uncharacterized negative feedback regulation, the duration period of ~15 min with reduced ATP levels may induce some proteins to form aggregates that last for generations.

Many neurodegenerative diseases, such as Alzheimer's, Huntington's, and Parkinson's diseases, are associated with protein aggregation (Eisele, Monteiro et al., 2015, Josefson et al., 2017). On the other hand, mitochondrial dysfunction and accompanying energy failure in nerve cells may result in many types of neurodegenerative diseases based on a large body of evidence (Haelterman, Yoon et al., 2014, Pathak et al., 2013). For example, previous studies demonstrated that ATP levels in the brain were decreased in patients with early Parkinson's disease (Mochel, N'Guyen et al., 2012) and also that ATP synthesis in the brain was not properly regulated in patients with early Huntington's disease (Hattingen, Magerkurth et al., 2009) and in the corresponding mouse model (Mochel, Durant et al., 2012). Therefore, protein aggregation induced by the ATP catastrophe, as revealed in the present study, may link energy failure and protein aggregation, providing a comprehensive insight into the onset of neurodegenerative diseases. Further studies are warranted to clarify whether the ATP catastrophe also occurs in the neurons of patients at risk of neurodegenerative diseases or in the elderly. However, neither biochemical measurements nor mass spectrometry is capable of detecting the ATP catastrophe because of their insufficient time and space resolution. Thus, an ATP imaging approach using the yeast model system will be the first choice for elucidating the molecular mechanisms underlying ATP homeostasis and ATP catastrophe-induced protein aggregation.

A recent study reported that the activation of AMPK by metformin ameliorated the progression of Huntington's disease in a mouse model (Arnoux, Willam et al., 2018), and the potential therapeutic use of metformin for neurodegenerative diseases is being discussed

(Rotermund, Machetanz et al., 2018). Furthermore, the involvement of ATP and ADKs in preventing the manifestation of Parkinson's disease in mouse models and patients has been proposed (Garcia-Esparcia, Hernandez-Ortega et al., 2015, Nakano, Imamura et al., 2017). Protein aggregation induced by the ATP catastrophe may be a general mechanism for the development of proteinopathies. The present study study using ATP imaging revealed a physiological consequence of a failure in ATP homeostasis in living cells for the first time and suggests that ATP homeostasis has potential as a target for preventing/treating neurodegenerative diseases.

MATERIALS AND METHODS

Yeast strains and plasmids

The budding yeast strains and plasmids used in the present study are listed in Supplementary Tables S1 and S2, respectively. These strains were constructed by a PCR-based method (Janke, Magiera et al., 2004) and genetic crosses. The yeast knockout strain collection was originally purchased from GE Healthcare (cat. # YSC1053).

Media and cell culture

The standard technique for the yeast culture and manipulation was used (Guthrie & Fink, 2002). Synthetic medium (SC) was prepared according to the recipe of Hanscho et al. (Hanscho, Ruckerbauer et al., 2012). 2-Deoxy-D-glucose (2DG), tunicamycin, and MG132 were purchased from FUJIFILM Wako (cat. # 046-06483, 202-08241, and 139-18451, respectively). Tunicamycin and MG132 were dissolved in dimethylsulfoxide (DMSO) to make stock solutions (5 mg/ml and 42 mM, respectively). Cells were grown to the mid-log phase at 30°C in SC before imaging unless otherwise noted.

Microscopy

Cells expressing Hsp104-GFP or GFP-Ubc9ts were concentrated by centrifugation and sandwiched between a slide and coverslip (No. 1.5 thickness, Matsunami, Osaka, Japan). Immobilized cells were imaged using an inverted fluorescent microscope (Eclipse Ti-E, Nikon) equipped with an Apo TIRF 100× Oil DIC N2/NA 1.49 objective lens and electron-multiplying charge-coupled device camera (iXon3 DU897E-CS0-#BV80, Andor) at approximately 25°C. The Hsp104-GFP and GFP-Ubc9ts fluorescent signal was collected from stacks of 11 *z*-sections spaced by 0.5 μm, and the maximum projections of the optical sections were shown in Figs. 4, 5, and S6. Cells expressing QUEEN were immobilized on a concanavalin A-coated 35-mm glass-bottomed dish (#3971-035, No. 1.5 thickness, IWAKI). The dish was filled with an excess amount of medium (4.5–5 ml) against the cell volume to minimize changes in the chemical compositions of the medium during observations. QUEEN fluorescence was acquired as previously described (Takaine et al., 2019). Cells expressing α-synuclein-GFP were immobilized on a slide glass as described above, and the fluorescence signal was collected from a single *z*-plane using an inverted fluorescent microscope (Eclipse Ti2-E, Nikon, Tokyo, Japan) equipped with a CFI Plan Apoλ100× Oil DIC/NA1.45 objective

lens and CMOS image sensor (DS-Qi2, Nikon). Images of cells were acquired from several fields of view for each experimental condition.

Data analysis

Numerical data were plotted using KaleidaGraph software ver. 4.5.1 (Synergy Software). Means, SDs, and *p* values were calculated using Excel software (Microsoft, WA, US). Significance between two sets of data was tested using the unpaired one-tailed Welch's *t*-test unless otherwise noted, and was indicated by an asterisk or *p* value. The horizontal bar in the dot plot indicates the average of each population. All measurements were repeated at least twice to confirm reproducibility.

ATP concentrations in yeast cells were estimated using QUEEN-based ratiometric imaging, as previously described (Takaine, 2019), (Takaine et al., 2019). The QUEEN ratio is proportional to ATP concentrations and pseudo-colored to reflect its value throughout the present study. The mean QUEEN ratio inside of a cell represents the intracellular ATP concentration of the cell.

The autocorrelation functions (ACF) of oscillations in the QUEEN ratio were calculated using R studio software ver. 3.4.1 (R Core Team, 2017). The apparent period of oscillation was estimated from the positive second peak of the correlation coefficient, which was outside the 95% confidence interval and significant ($p < 0.05$), rejecting the assumption that there is no correlation.

ACKNOWLEDGMENTS

We are grateful to the Yeast Genetic Resource Center, Y. Ohya, K. Ohashi, H. Takagi, D. Watanabe, and J. Frydman for providing the yeast strains and plasmids. We thank the members of the Yoshida/Takaine labs for their support. This work was supported by JSPS grants 16H04781 (S.Y. and M.T.) and 15K18525 (M.T.) and the Takeda Science foundation (S.Y.). This work was also supported by the joint research program of the Institute for Molecular and Cellular Regulation, Gunma University, Japan.

AUTHOR CONTRIBUTIONS

M.T. and S.Y. conceived and designed the project. M.T. conducted experiments and the data analysis. H.I. provided a key reagent and expertise. M.T. and S.Y wrote the manuscript with input from H.I.

CONFLICT OF INTEREST

The authors declare no competing interests.

REFERENCES

Arnoux I, Willam M, Griesche N, Krummeich J, Watari H, Offermann N, Weber S, Narayan Dey P, Chen C, Monteiro O, Buettner S, Meyer K, Bano D, Radyushkin K, Langston R, Lambert JJ, Wanker E, Methner A, Krauss S, Schweiger S et al. (2018) Metformin reverses early cortical network dysfunction and behavior changes in Huntington's disease. *Elife* 7

Baryshnikova A (2016) Systematic Functional Annotation and Visualization of Biological Networks. *Cell Syst* 2: 412-21

Benaroudj N, Zwickl P, Seemuller E, Baumeister W, Goldberg AL (2003) ATP hydrolysis by the proteasome regulatory complex PAN serves multiple functions in protein degradation. *Mol Cell* 11: 69-78

Bhat AH, Dar KB, Anees S, Zargar MA, Masood A, Sofi MA, Ganie SA (2015) Oxidative stress, mitochondrial dysfunction and neurodegenerative diseases; a mechanistic insight. *Biomed Pharmacother* 74: 101-10

Carlson M (1999) Glucose repression in yeast. *Curr Opin Microbiol* 2: 202-7

Cherry JM, Hong EL, Amundsen C, Balakrishnan R, Binkley G, Chan ET, Christie KR, Costanzo MC, Dwight SS, Engel SR, Fisk DG, Hirschman JE, Hitz BC, Karra K, Krieger CJ, Miyasato SR, Nash RS, Park J, Skrzypek MS, Simison M et al. (2012) Saccharomyces Genome Database: the genomics resource of budding yeast. *Nucleic Acids Res* 40: D700-5

Daignan-Fornier B, Fink GR (1992) Coregulation of purine and histidine biosynthesis by the transcriptional activators BAS1 and BAS2. *Proc Natl Acad Sci U S A* 89: 6746-50

Denis V, Boucherie H, Monribot C, Daignan-Fornier B (1998) Role of the myb-like protein bas1p in Saccharomyces cerevisiae: a proteome analysis. *Mol Microbiol* 30: 557-66

Edelman AM, Blumenthal DK, Krebs EG (1987) Protein serine/threonine kinases. *Annu Rev Biochem* 56: 567-613

Eftekharzadeh B, Hyman BT, Wegmann S (2016) Structural studies on the mechanism of protein aggregation in age related neurodegenerative diseases. *Mech Ageing Dev* 156: 1-13

Eisele YS, Monteiro C, Fearns C, Encalada SE, Wiseman RL, Powers ET, Kelly JW (2015) Targeting protein aggregation for the treatment of degenerative diseases. *Nat Rev Drug Discov* 14: 759-80

Garcia-Esparcia P, Hernandez-Ortega K, Ansoleaga B, Carmona M, Ferrer I (2015) Purine metabolism gene deregulation in Parkinson's disease. *Neuropathol Appl Neurobiol* 41: 926-40

Gauthier S, Coulpier F, Jourdren L, Merle M, Beck S, Konrad M, Daignan-Fornier B, Pinson B (2008) Co-regulation of yeast purine and phosphate pathways in response to adenylic nucleotide variations. *Mol Microbiol* 68: 1583-94

Ghillebert R, Swinnen E, Wen J, Vandesteene L, Ramon M, Norga K, Rolland F, Winderickx J (2011) The AMPK/SNF1/SnRK1 fuel gauge and energy regulator: structure, function and regulation. *FEBS J* 278: 3978-90

Guthrie C, Fink GR (2002) *Guide to yeast genetics and molecular and cell Biology: Part C*. Gulf Professional

497 Publishing,
498 Haelterman NA, Yoon WH, Sandoval H, Jaiswal M, Shulman JM, Bellen HJ (2014) A Mitocentric View of
499 Parkinson's Disease. *Annu Rev Neurosci* 37: 137-159
500 Hanscho M, Ruckerbauer DE, Chauhan N, Hofbauer HF, Krahulec S, Nidetzky B, Kohlwein SD, Zanghellini
501 J, Natter K (2012) Nutritional requirements of the BY series of Saccharomyces cerevisiae strains for optimum
502 growth. *FEMS Yeast Res* 12: 796-808
503 Hardie DG, Carling D, Carlson M (1998) The AMP-activated/SNF1 protein kinase subfamily: metabolic
504 sensors of the eukaryotic cell? *Annu Rev Biochem* 67: 821-55
505 Hardie DG, Schaffer BE, Brunet A (2016) AMPK: An Energy-Sensing Pathway with Multiple Inputs and
506 Outputs. *Trends Cell Biol* 26: 190-201
507 Hattingen E, Magerkurth J, Pilatus U, Mozer A, Seifried C, Steinmetz H, Zanella F, Hilker R (2009)
508 Phosphorus and proton magnetic resonance spectroscopy demonstrates mitochondrial dysfunction in early and
509 advanced Parkinson's disease. *Brain* 132: 3285-97
510 Hayes MH, Peuchen EH, Dovichi NJ, Weeks DL (2018) Dual roles for ATP in the regulation of phase
511 separated protein aggregates in Xenopus oocyte nucleoli. *eLife* 7: e35224
512 Hedbacker K, Carlson M (2008) SNF1/AMPK pathways in yeast. *Front Biosci* 13: 2408-20
513 Herzig S, Shaw RJ (2017) AMPK: guardian of metabolism and mitochondrial homeostasis. *Nat Rev Mol Cell*
514 *Biol* 19: 121
515 Hoyle NP, Castelli LM, Campbell SG, Holmes LE, Ashe MP (2007) Stress-dependent relocalization of
516 translationally primed mRNPs to cytoplasmic granules that are kinetically and spatially distinct from P-bodies. *J*
517 *Cell Biol* 179: 65-74
518 Jain S, Wheeler JR, Walters RW, Agrawal A, Barsic A, Parker R (2016) ATPase-Modulated Stress Granules
519 Contain a Diverse Proteome and Substructure. *Cell* 164: 487-98
520 Janke C, Magiera MM, Rathfelder N, Taxis C, Reber S, Maekawa H, Moreno-Borchart A, Doenges G,
521 Schwob E, Schiebel E, Knop M (2004) A versatile toolbox for PCR-based tagging of yeast genes: new
522 fluorescent proteins, more markers and promoter substitution cassettes. *Yeast* 21: 947-62
523 Janssen E, Dzeja PP, Oerlemans F, Simonetti AW, Heerschap A, de Haan A, Rush PS, Terjung RR, Wieringa
524 B, Terzic A (2000) Adenylate kinase 1 gene deletion disrupts muscle energetic economy despite metabolic
525 rearrangement. *EMBO J* 19: 6371-81
526 Jiang H, Poirier MA, Ross CA (2005) A structure-based analysis of huntingtin mutant polyglutamine
527 aggregation and toxicity: evidence for a compact beta-sheet structure. *Hum Mol Genet* 14: 765-774
528 Josefson R, Andersson R, Nyström T (2017) How and why do toxic conformers of aberrant proteins
529 accumulate during ageing? *Essays Biochem* 61: 317
530 Kaganovich D, Kopito R, Frydman J (2008) Misfolded proteins partition between two distinct quality control
531 compartments. *Nature* 454: 1088-95

Kruegel U, Robison B, Dange T, Kahlert G, Delaney JR, Kotireddy S, Tsuchiya M, Tsuchiyama S, Murakami CJ, Schleit J, Sutphin G, Carr D, Tar K, Dittmar G, Kaeberlein M, Kennedy BK, Schmidt M (2011) Elevated proteasome capacity extends replicative lifespan in Saccharomyces cerevisiae. *PLoS Genet* 7: e1002253

Lashuel HA, Overk CR, Oueslati A, Masliah E (2013) The many faces of alpha-synuclein: from structure and toxicity to therapeutic target. *Nat Rev Neurosci* 14: 38-48

Ljungdahl PO, Daignan-Fornier B (2012) Regulation of amino acid, nucleotide, and phosphate metabolism in Saccharomyces cerevisiae. *Genetics* 190: 885-929

Meriin AB, Zhang X, He X, Newnam GP, Chernoff YO, Sherman MY (2002) Huntington toxicity in yeast model depends on polyglutamine aggregation mediated by a prion-like protein Rnq1. *J Cell Biol* 157: 997-1004

Mochel F, Durant B, Meng X, O'Callaghan J, Yu H, Brouillet E, Wheeler VC, Humbert S, Schiffmann R, Durr A (2012) Early alterations of brain cellular energy homeostasis in Huntington disease models. *J Biol Chem* 287: 1361-70

Mochel F, N'Guyen TM, Deelchand D, Rinaldi D, Valabregue R, Wary C, Carlier PG, Durr A, Henry PG (2012) Abnormal response to cortical activation in early stages of Huntington disease. *Mov Disord* 27: 907-10

Mortensen SP, Thaning P, Nyberg M, Saltin B, Hellsten Y (2011) Local release of ATP into the arterial inflow and venous drainage of human skeletal muscle: insight from ATP determination with the intravascular microdialysis technique. *The Journal of Physiology* 589: 1847-1857

Nakano M, Imamura H, Sasaoka N, Yamamoto M, Uemura N, Shudo T, Fuchigami T, Takahashi R, Kakizuka A (2017) ATP Maintenance via Two Types of ATP Regulators Mitigates Pathological Phenotypes in Mouse Models of Parkinson's Disease. *EBioMedicine* 22: 225-241

Outeiro TF, Lindquist S (2003) Yeast cells provide insight into alpha-synuclein biology and pathobiology. *Science* 302: 1772-5

Patel A, Malinovska L, Saha S, Wang J, Alberti S, Krishnan Y, Hyman AA (2017) ATP as a biological hydrotrope. *Science* 356: 753-756

Pathak D, Berthet A, Nakamura K (2013) Energy failure: does it contribute to neurodegeneration? *Ann Neurol* 74: 506-16

Piotrowski JS, Li SC, Deshpande R, Simpkins SW, Nelson J, Yashiroda Y, Barber JM, Safizadeh H, Wilson E, Okada H, Gebre AA, Kubo K, Torres NP, LeBlanc MA, Andrusiak K, Okamoto R, Yoshimura M, DeRango-Adem E, van Leeuwen J, Shirahige K et al. (2017) Functional annotation of chemical libraries across diverse biological processes. *Nature Chemical Biology* 13: 982

R Core Team (2017) R: A Language and Environment for Statistical Computing. In Vienna, Austria: R Foundation for Statistical Computing

Rotermund C, Machetanz G, Fitzgerald JC (2018) The Therapeutic Potential of Metformin in Neurodegenerative Diseases. *Front Endocrinol (Lausanne)* 9: 400

Sharma N, Brandis KA, Herrera SK, Johnson BE, Vaidya T, Shrestha R, DebBurman SK (2006) α-synuclein budding yeast model. *J Mol Neurosci* 28: 161-178

Sridharan S, Kurzawa N, Werner T, Günthner I, Helm D, Huber W, Bantscheff M, Savitski MM (2019) Proteome-wide solubility and thermal stability profiling reveals distinct regulatory roles for ATP. *Nature Communications* 10: 1155

Takaine M (2019) QUEEN-based Spatiotemporal ATP Imaging in Budding and Fission Yeast. *Bio-protocol* 9: e3320

Takaine M, Ueno M, Kitamura K, Imamura H, Yoshida S (2019) Reliable imaging of ATP in living budding and fission yeast. *J Cell Sci* 132

Tanaka K, Waxman L, Goldberg AL (1983) ATP serves two distinct roles in protein degradation in reticulocytes, one requiring and one independent of ubiquitin. *J Cell Biol* 96: 1580-5

Tofaris GK, Kim HT, Hourez R, Jung JW, Kim KP, Goldberg AL (2011) Ubiquitin ligase Nedd4 promotes alpha-synuclein degradation by the endosomal-lysosomal pathway. *Proc Natl Acad Sci U S A* 108: 17004-9

Usaj M, Tan Y, Wang W, VanderSluis B, Zou A, Myers CL, Costanzo M, Andrews B, Boone C (2017) TheCellMap.org: A Web-Accessible Database for Visualizing and Mining the Global Yeast Genetic Interaction Network. *G3 (Bethesda)* 7: 1539-1549

Wijayanti I, Watanabe D, Oshiro S, Takagi H (2015) Isolation and functional analysis of yeast ubiquitin ligase Rsp5 variants that alleviate the toxicity of human α-synuclein. *The Journal of Biochemistry* 157: 251-260

Willingham S, Outeiro TF, DeVit MJ, Lindquist SL, Muchowski PJ (2003) Yeast genes that enhance the toxicity of a mutant huntingtin fragment or alpha-synuclein. *Science* 302: 1769-72

Wilson WA, Hawley SA, Hardie DG (1996) Glucose repression/derepression in budding yeast: SNF1 protein kinase is activated by phosphorylation under derepressing conditions, and this correlates with a high AMP:ATP ratio. *Curr Biol* 6: 1426-34

Xiao B, Heath R, Saiu P, Leiper FC, Leone P, Jing C, Walker PA, Haire L, Eccleston JF, Davis CT, Martin SR, Carling D, Gamblin SJ (2007) Structural basis for AMP binding to mammalian AMP-activated protein kinase. *Nature* 449: 496-500

Xie Y, Varshavsky A (2001) RPN4 is a ligand, substrate, and transcriptional regulator of the 26S proteasome: a negative feedback circuit. *Proc Natl Acad Sci U S A* 98: 3056-61

Yaginuma H, Kawai S, Tabata KV, Tomiyama K, Kakizuka A, Komatsuzaki T, Noji H, Imamura H (2014) Diversity in ATP concentrations in a single bacterial cell population revealed by quantitative single-cell imaging. *Sci Rep* 4: 6522

FIGURE LEGENDS

Fig. 1 AMPK is involved in the maintenance of cellular ATP levels in non-starving cells

(A) Visualization of intracellular ATP levels in wild-type (WT) and *snf1Δ* cells using the ATP sensor QUEEN. Cells were grown to the mid-log phase in SC-H medium containing the indicated concentrations of glucose and then imaged. White scale bar = 5 μm. (B) *snf1Δ* cells had lower ATP levels than wild-type cells. The mean QUEEN ratio inside a single cell (mean QUEEN ratio/cell), which represents the intracellular ATP level of the cell, was quantified for each cell from the ratio image. Data are the mean of the cell population ± 1SD (error bar) normalized to wild-type cells. N = 105–193 cells were scored. Asterisks indicate a significant difference from WT ($p < 0.05$). (C) ATP levels in single-deletion mutants of AMPK *β* subunits. Data are the mean of the cell population ± 1SD (error bar) normalized to wild-type cells. N = 177–223 cells were scored. Asterisks indicate a significant difference between the two strains (*, $p < 0.05$; **, $p < 0.01$). N.S., no significance. (D) *mig1Δ* cells had slightly lower ATP levels than wild-type cells. Data are the mean of the cell population ± 1SD (error bar) normalized to wild-type cells. N = 190–231 cells were scored. Asterisks indicate a significant difference between the two strains.

Fig. 2 Interconversion and active synthesis of adenine nucleotides are important for ATP homeostasis

(A) Adk1 and Snf1 synergistically control cellular ATP levels. QUEEN ratio images of ATP homeostasis mutant cells grown in the medium containing 2% glucose. The asterisk indicates an example of cells with significantly reduced ATP levels. (B) Mean QUEEN ratios of cells were translated to ATP concentrations and shown in a dot plot. The horizontal bar indicates the mean of each population. Asterisks indicate *p* values versus WT: *=1.5×10^{-59}, **=2.3×10^{-34}, ***=2.9×10^{-117}. CV: coefficient of variance. N = 134–276 cells were scored. (C) QUEEN ratio images of *bas1Δ* cells grown in the 2% glucose medium. Growth in media supplemented with 0.11 mg/ml adenine partially restored the low ATP phenotype of *bas1*Δ. (D) The ATP concentrations of cells shown in (C) were plotted. Asterisks indicate *p* values: *=2.3×10^{-160}, **=8.8×10^{-12} (versus WT in glucose), ***=3.6×10^{-20} (versus *bas1*Δ in glucose). CV: coefficient of variance. N = 186–296 cells were scored.

Fig. 3 Temporal fluctuations in ATP levels in *snf1*Δ*adk1*Δ and *bas1*Δ cells

(A, C) Time-lapse imaging of QUEEN in *snf1*Δ *adk1*Δ cells in the 2% glucose medium. Images at the representative time points were shown. The QUEEN ratio decreased twice (indicated by arrowheads) within a short interval. See also Movie S1. Data were converted

into ATP concentrations and plotted in (C). (B, D) Another example of time-lapse imaging of QUEEN in *snf1*Δ*adk1*Δ cells in the 2% glucose medium. The QUEEN ratio decreased twice (indicated by arrowheads) with a long interval. See also Movie S2. Data were converted into ATP concentrations and plotted in (D). (E) Time-lapse imaging of QUEEN in *bas1*Δ in the 2% glucose medium. The ATP concentrations of the mother (cell-1) and daughter (cell-2) were plotted at the bottom. Images at the representative time points were shown on the top. Note that the QUEEN ratio is synchronized until cells undergo separation at the time point of 76 min indicated by an arrow. After separation, each cell has a unique periodic cycle of ATP. The movie is available in Movie S3. White scale bar = 5 μm.

Fig. 4 ATP homeostasis is required to prevent protein aggregation

(A) Functional landscape of known interactors of ATP mutants. Negative genetic interactors of the indicated gene were derived from the SGD database (https://www.yeastgenome.org/) (Cherry, Hong et al., 2012) and overlaid on a functional map based on the global genetic interaction network of the yeast genome (Baryshnikova, 2016, Usaj et al., 2017). *URA6* encodes an uridylate kinase that is essential for viability, which also exhibits adenylate kinase activity. (B) Each strain of the indicated genotype was serially diluted (five-fold), spotted on the SC + 2% glucose medium, and grown under the indicated stress conditions. Photos were taken after 2-3 days. (C) Formation of Hsp104-GFP foci in ATP homeostasis mutants. The GFP signal (inverted grayscale) was imaged in the log phase culture of the indicated mutant cells expressing Hsp104-GFP at 35°C. (D) Quantification of data shown in (C). Data from similar experiments using strains expressing Pab1-GFP, instead of Hsp104-GFP, were also plotted. Values are the mean ± 1SD (error bars). Asterisks indicate a significant difference from WT ($p < 0.05$) (N=3–4). White scale bar = 5 μm.

Fig. 5 ATP depletion triggers protein aggregation in living yeast cells

(A) The formation of Hsp104-GFP foci after ATP depletion. Wild-type cells expressing Hsp104-GFP were grown to the log phase at 35°C in the medium containing 2% glucose. At the time point of 0 min, the medium was replaced with 20 mM 2DG (red) or 2% glucose (as a control; blue). Cells were released back to media containing 2% glucose at the time point of 50 min. Cells were imaged at the indicated time points, classified, and scored according to the number of Hsp104-GFP foci. Values are the mean (N = 3). Asterisks indicate a significant difference from the 2% glucose treatment ($p < 0.05$). (B) Representative images of cells analyzed in (A). (C) Formation of Ubc9-ts foci after ATP depletion. Cells expressing GFP-Ubc9-ts under an inducible *GAL* promoter were grown in the medium containing 2%

669 galactose (SC-gal) at 33°C, and the medium was then exchanged with 2DG or SC-gal. After
670 30 min, cells were imaged and scored for the number of GFP-Ubc9-ts foci. Representative
671 images (inverted grayscale) are shown on the left and summarized on the right. Values are the
672 mean ± 1SD (error bars) (N = 4). White scale bar = 5 μm.
673
674 Fig. 6 Aggregation and cytotoxicity of α-synuclein depends on ATP homeostasis
675 (A) Each strain of the indicated genotype was transformed with an expression vector carrying
676 α-synuclein-GFP or GFP, serially diluted (five-fold), spotted on SC + 2% galactose plates,
677 and then grown at 30°C for 3 days. (B) The localization of α-synuclein-GFP in ATP mutants.
678 Cells were grown on galactose plates at 30°C for more than 42 h and then imaged.
679 Representative images of α-synuclein-GFP (inverted grayscale) are shown. (C) Quantification
680 of the data shown in (B). Cells were classified and scored for the localization pattern of
681 α-synuclein-GFP. The percentage of cells showing α-synuclein-GFP foci are plotted. Data are
682 the mean ± 1SD (error bars) from 3–6 independent observations. N = 33–380 cells were
683 scored in each measurement. *P* values versus WT are shown. N.S., no significance (*p* value >
684 0.05). (D) *(top)* Each strain of the indicated genotype was transformed with an expression
685 vector carrying α-synuclein-GFP and grown on galactose plates containing 0 mM (−
686 Adenine) or 0.3 mM (+ Adenine) adenine at 30°C for 3 days. *(bottom)* Cells were grown on
687 galactose plates in the absence or presence of adenine at 30°C for 41-45 h and then imaged.
688 The percentage of cells showing α-synuclein-GFP foci were plotted. Data are the mean ± 1SD
689 (error bars) from 5 independent transformants. N = 53–258 cells were scored in each
690 measurement. *P* values versus "– Adenine" are shown. (E) Each strain of the indicated
691 genotype was serially diluted (five-fold), spotted on the SC + 2% glucose medium, and grown
692 under the indicated stress conditions. (F) Cells of the drug-sensitive strain Y13206 were
693 grown to the log phase at 37°C in the medium containing 2% glucose and supplemented with
694 0.1% DMSO or 0.1% DMSO plus 42 μM MG132 at $t = -30$ min. At $t = 0$ min, these cells
695 were washed and released in the medium containing 20 mM 2DG ± MG132, and the cells
696 were then washed and released again in the medium containing 2% glucose ± MG132. Cells
697 were imaged at the indicated time points and scored for the number of Hsp104-GFP foci.
698 Data are the mean ± 1SD (error bars). Asterisks indicate a significant difference from DMSO
699 ($p < 0.02$) (N=3).
700
701 Fig. 7 Models for ATP homeostasis and its role in proteostasis
702 (A) Schematic summary of the roles of Snf1, Adk1, and Bas1 in ATP homeostasis. (B) A
703 schematic model for ATP homeostasis preventing cytotoxic protein aggregation.

SUPPLEMENTARY INFORMATION

Supplementary figure legends

Fig. S1 Adenylate kinase Adk1 is involved in the maintenance of cellular ATP concentrations

(A) QUEEN ratio images of wild-type and *adk1Δ* cells grown in 2% glucose or 2% galactose. White scale bar = 5 μm. (B) Quantification of data shown in (A). The mean QUEEN ratio/cell was quantified for each cell from ratio images. Values are the mean of the cell population ± 1SD (error bar). N = 182–236 cells were scored. Asterisks indicate a significant difference from WT ($p < 0.05$).

Fig. S2 ATP levels in *bas1*Δ *snf1*Δ cells

(A) QUEEN ratio images of wild-type, *bas1Δ*, *snf1Δ*, and *bas1Δ snf1Δ* cells. (B) Quantification of data shown in (A). The mean QUEEN ratio/cell was quantified for each cell from ratio images. Data are shown as a dot plot. The horizontal bar in the plot indicates the mean of each population. Significance between two sets of data was tested using the unpaired two-tailed Welch's *t*-test and indicated by *p* values. N.S., no significance (*p*-value > 0.05).

Fig. S3 Time-lapse imaging of QUEEN in *snf1*Δ *adk1*Δ cells

Time-lapse imaging of QUEEN in *snf1*Δ *adk1*Δ cells in the 2% glucose medium. An example of *snf1*Δ *adk1*Δ cell showing an irreversible decrease in the QUEEN ratio (indicated by an arrowhead). In this case, the cell eventually died (indicated by an arrow). Images at the representative time points were shown. The ATP concentration was plotted at the bottom. White scale bar = 5 μm.

Fig. S4. Oscillatory behavior of the ATP concentration visualized in *bas1*Δ cells

(A) Another example of *bas1Δ* cells showing an oscillating QUEEN ratio. In this case, cytokinesis had just been completed at t = 0 min. ATP concentrations in cell-1 and cell-2 were plotted at the bottom. See also Movie S4. White scale bar = 5 μm. (B) Autocorrelation function of the QUEEN ratio calculated from the data on cell-1 in Fig. 3E. Blue dotted lines indicate the 95% confidence interval. An arrow indicates the second peak of the correlation and corresponds to the apparent period.

Fig. S5 *In silico* analysis of interactors of ATP mutants

Genetic and physical interactors of the indicated genes were derived from the SGD database (https://www.yeastgenome.org/) (Cherry et al., 2012) and overlaid on a functional map based

on the global genetic interaction network of the yeast genome (Baryshnikova, 2016, Usaj et al., 2017). *URA6* encodes an uridylate kinase essential for viability, which also exhibits adenylate kinase activity.

Fig. S6 Simultaneous observation of Hsp104 and Pab1 foci

Wild-type cells expressing Hsp104-GFP and Pab1-RedStar2 were grown to the log phase at 37°C in the medium containing 2% glucose. Cells were washed and released either in the medium containing 20 mM 2DG (top) or in the medium lacking glucose (bottom), and then imaged after 30 and 60 min. White scale bar = 5 μm.

Fig. S7 Cytotoxicity of polyQ containing the huntingtin protein in wild-type and ATP-mutant yeast cells

Each strain of the indicated genotype was transformed with an expression vector carrying Htt103Q and grown on glucose ((-), no induction) or raffinose ((+), leaky expression) plates at 30°C for 3 days.

755 Table S1. *Strains used in the present study*

Name	Genotype	Source	Figure
MTY3008	*snf1Δ::kanMX6 leu2Δ0 lys2Δ0 ura3Δ0*	Lab stock	4B, 6A-C, 6E, S7
MTY3015	*his3Δ1 leu2Δ0 lys2Δ0 ura3Δ0*	Lab stock	4B, 6A-E, S7
MTY3049	*adk1Δ::kanMX6 his3Δ1 leu2Δ0 lys2Δ0 ura3Δ0*	Lab stock	4B, 6A-E, S7
MTY3118	*bas1Δ::kanMX6 leu2Δ0 lys2Δ0 ura3Δ0*	Lab stock	4B, 6A-E, S7
MTY3143	*his3Δ1:: 2×pRS303-P_{TEF}-QUEEN-2m-T_{CYC1} leu2Δ0 lys2Δ0 ura3Δ0*	This study	S1
MTY3149	*adk1Δ::kanMX6 his3Δ1:: 2×pRS303-P_{TEF}-QUEEN-2m-T_{CYC1} leu2Δ0 lys2Δ0 ura3Δ0*	This study	S1
MTY3264	*his3Δ1:: 3×pRS303-P_{TEF}-QUEEN-2m-T_{CYC1} leu2Δ0 lys2Δ0 ura3Δ0 MYO1-3mCherry-hphMX6*	Takaine et al., 2019	2A, B, S2
MTY3270	*bas1Δ::kanMX6 his3Δ1:: 3×pRS303-P_{TEF}-QUEEN-2m-T_{CYC1} leu2Δ0 lys2Δ0 ura3Δ0 MYO1-3mCherry-hphMX6*	This study	2C, D, 3E, S2, S4
MTY3293	*adk1Δ::kanMX6 his3Δ1:: 3×pRS303-P_{TEF}-QUEEN-2m-T_{CYC1} leu2Δ0 lys2Δ0 ura3Δ0 MYO1-3mCherry-hphMX6*	This study	2A, B
MTY3355	*adk1Δ::kanMX6 snf1Δ::natNT2 his3Δ1:: 3×pRS303-P_{TEF}-QUEEN-2m-T_{CYC1} leu2Δ0 lys2Δ0 ura3Δ0 MYO1-3mCherry-hphMX6*	This study	2A, B, 3A-D, S3
MTY3371	*snf1Δ::kanMX6 his3Δ1:: 3×pRS303-P_{TEF}-QUEEN-2m-T_{CYC1} leu2Δ0 lys2Δ0 ura3Δ0 MYO1-3mCherry-hphMX6*	This study	2A, B, S2
MTY3412	*adk1Δ::kanMX6 snf1Δ::natNT2 leu2Δ0 lys2Δ0 ura3Δ0*	This study	4B, 6A-E, S7
MTY3420	*Hsp104-yeGFP-hphNT1 his3Δ1 leu2Δ0 lys2Δ0 ura3Δ0*	This study	4C, D, 5A, B
MTY3421	*snf1Δ::kanMX6 Hsp104-yeGFP-hphNT1 his3Δ1 leu2Δ0 lys2Δ0 ura3Δ0*	This study	4C, D
MTY3422	*bas1Δ::kanMX6 Hsp104-yeGFP-hphNT1 his3Δ1 leu2Δ0 lys2Δ0 ura3Δ0*	This study	4C, D
MTY3424	*adk1Δ::kanMX6 Hsp104-yeGFP-hphNT1 his3Δ1 leu2Δ0 lys2Δ0 ura3Δ0*	This study	4C-D
MTY3425	*adk1Δ::kanMX6 snf1Δ::natNT2 Hsp104-yeGFP-hphNT1 his3Δ1 leu2Δ0 lys2Δ0 ura3Δ0*	This study	4C, D
MTY3489	*atg1Δ::kanMX6 his3Δ1 leu2Δ0 lys2Δ0 ura3Δ0*	Lab stock	6E
MTY3493	*snq2Δ::KILeu2; pdr3Δ::KIura3; pdr1Δ::natMX4; can1Δ::STE2prSp_his5 lyp1Δ*	From Y.	Parental

	his3Δ1 leu2Δ0 ura3Δ0 met15Δ0 LYS2+	Ohya, (Piotrowski et al., 2017)	strain of MTY3501
MTY3501	*Hsp104-yeGFP-hphNT1 snq2Δ::KILeu2; pdr3Δ::KIura3; pdr1Δ::natMX4; can1Δ::STE2prSp_his5 lyp1Δ his3Δ1 leu2Δ0 ura3Δ0 met15Δ0 LYS2+*	This study	6F
MTY3503	*Pab1- yeGFP-hphNT1 his3Δ1 leu2Δ0 lys2Δ0 ura3Δ0*	This study	4D
MTY3504	*Hsp104-yeGFP-hphNT1 Pab1-RedStar2-natNT2 his3Δ1 leu2Δ0 lys2Δ0 ura3Δ0*	This study	S6
MTY3505	*snf1Δ::kanMX6 Pab1- yeGFP-hphNT1 his3Δ1 leu2Δ0 lys2Δ0 ura3Δ0*	This study	4D
MTY3506	*adk1Δ::kanMX6 Pab1- yeGFP-hphNT1 his3Δ1 leu2Δ0 lys2Δ0 ura3Δ0*	This study	4D
MTY3507	*adk1Δ::kanMX6 snf1Δ::natNT2 Pab1- yeGFP-hphNT1 his3Δ1 leu2Δ0 lys2Δ0 ura3Δ0*	This study	4D
MTY3508	*bas1Δ::kanMX6 Pab1- yeGFP-hphNT1 his3Δ1 leu2Δ0 lys2Δ0 ura3Δ0*	This study	4D
MTY3513	*atg1Δ::natNT2 adk1Δ::kanMX6 his3Δ1 leu2Δ0 lys2Δ0 ura3Δ0*	This study	6E
MTY3514	*atg1Δ::natNT2 snf1Δ::kanMX6 his3Δ1 leu2Δ0 lys2Δ0 ura3Δ0*	This study	6E
MTY3515	*atg1Δ::natNT2 bas1Δ::kanMX6 his3Δ1 leu2Δ0 lys2Δ0 ura3Δ0*	This study	6E
MTY3516	*rpn4Δ::natNT2 adk1Δ::kanMX6 his3Δ1 leu2Δ0 lys2Δ0 ura3Δ0*	This study	6E
MTY3517	*rpn4Δ::natNT2 snf1Δ::kanMX6 his3Δ1 leu2Δ0 lys2Δ0 ura3Δ0*	This study	6E
MTY3518	*rpn4Δ::natNT2 bas1Δ::kanMX6 his3Δ1 leu2Δ0 lys2Δ0 ura3Δ0*	This study	6E
MTY3525	*rpn4Δ::kanMX6 his3Δ1 leu2Δ0 lys2Δ0 ura3Δ0*	Lab stock	6A-C, 6E

756

757 Table S2. *Plasmids used in the present study*

Name	Structure	Source	Purpose
MTP3091	pESC-Leu-GFP-Ubc9-ts	Judith Frydman (pJF1089)	Fig. 5C
MTP3088	p426 103Q GAL	Addgene (cat.# 1188)	Fig. S7
MTP3108	pYES2-α-synuclein-GFP	H. Takagi (Wijayanti et al., 2015)	Fig. 6A-D
MTP3090	pYES2-GFP	K. Ohashi	Fig. 6A

Captions for supplementary movies

Movie S1

Time-lapse imaging of QUEEN in *snf1*Δ*adk1*Δ cells in the 2% glucose medium. Corresponding to the data shown in Fig. 3A. The QUEEN ratio decreased twice (116 and 132 min) within a short interval. White scale bar = 5 μm.

Movie S2

Another example of *snf1*Δ*adk1*Δ cells showing a sudden decrease in the QUEEN ratio. Corresponding to the data shown in Fig. 3B. The QUEEN ratio decreased twice (180 and 356 min) with a long interval. White scale bar = 5 μm.

Movie S3

Oscillatory behavior of the QUEEN ratio in *bas1*Δ cells. Corresponding to the data shown in Fig. 3E. Left, the QUEEN ratio image; middle, Myo1-mCherry (inverted grayscale image); right, bright field image. Images were taken every 4 min. White scale bar = 5 μm.

Movie S4

Another example of *bas1*Δ cells showing an oscillating QUEEN ratio. Corresponding to the data shown in Supplementary Fig. S4A. Left, the QUEEN ratio image; right, bright field image. In this case, cytokinesis had already been completed at t = 0 min. Images were taken every 3 min. White scale bar = 5 μm.

Fig. 1

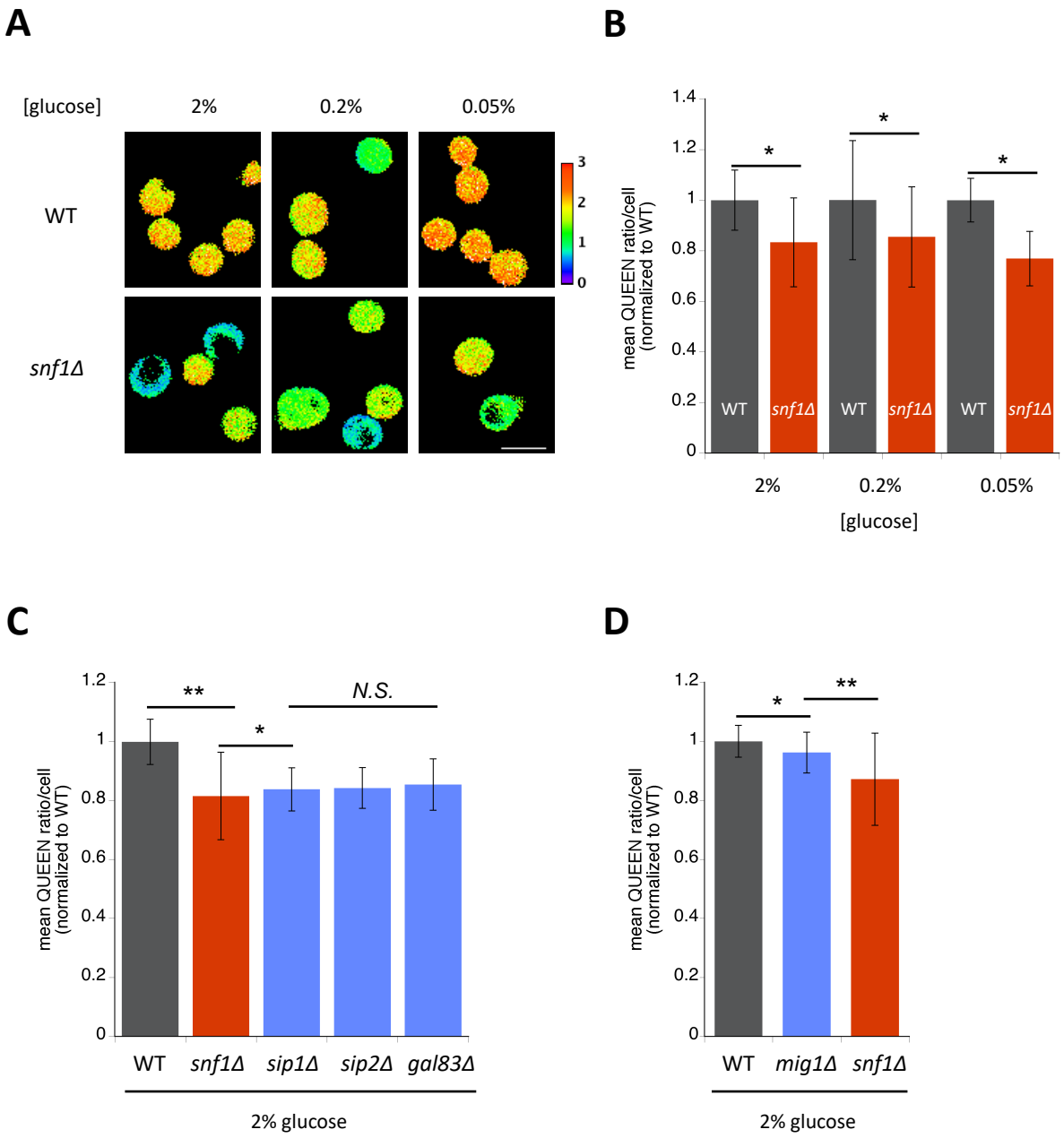
A
[glucose]
2%
0.2%
0.05%
WT
snf1Δ
3
2
1
0
B
mean QUEEN ratio/cell
(normalized to WT)
1.4
1.2
1
0.8
0.6
0.4
0.2
0
*
*
*
WT
snf1Δ
WT
snf1Δ
WT
snf1Δ
2%
0.2%
0.05%
[glucose]
C
mean QUEEN ratio/cell
(normalized to WT)
1.2
1
0.8
0.6
0.4
0.2
0
**
*
N.S.
WT
snf1Δ
sip1Δ
sip2Δ
gal83Δ
2% glucose
D
mean QUEEN ratio/cell
(normalized to WT)
1.2
1
0.8
0.6
0.4
0.2
0
*
**
WT
mig1Δ
snf1Δ
2% glucose

Fig. 2

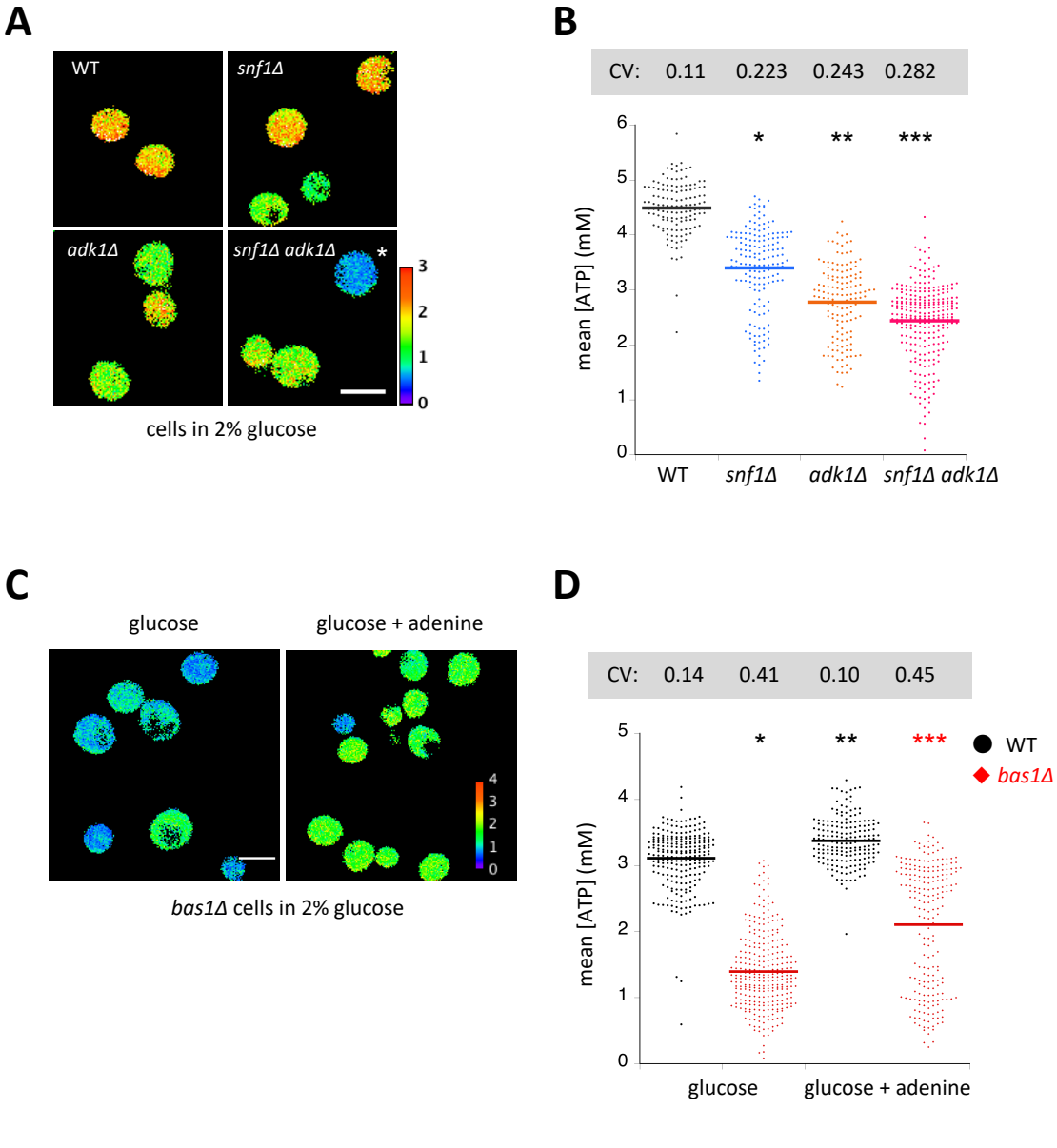
A
WT
snf1Δ
adk1Δ
snf1Δ adk1Δ
*
3
2
1
0
cells in 2% glucose
B
CV: 0.11 0.223 0.243 0.282
mean [ATP] (mM)
6
5
4
3
2
1
0
*
**
***
WT
snf1Δ
adk1Δ
snf1Δ adk1Δ
C
glucose
glucose + adenine
4
3
2
1
0
bas1Δ cells in 2% glucose
D
CV: 0.14 0.41 0.10 0.45
mean [ATP] (mM)
5
4
3
2
1
0
*
**
***
WT
bas1Δ
glucose
glucose + adenine

Fig. 3

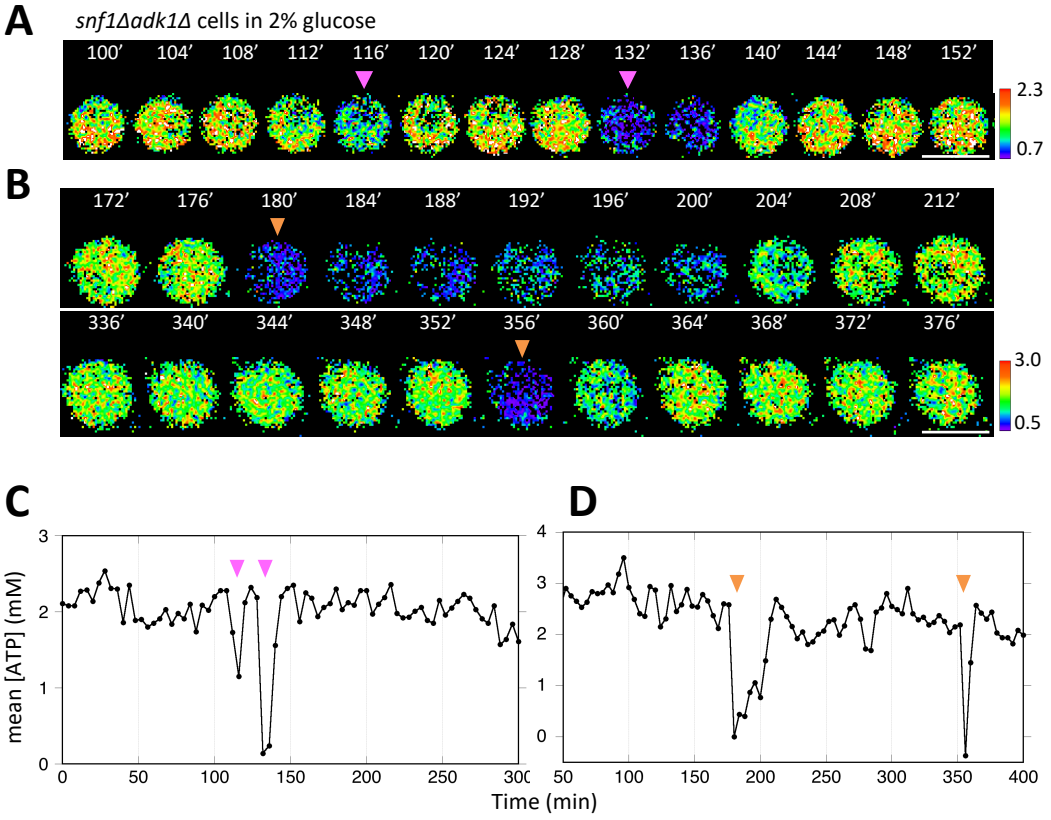
A
snf1Δadk1Δ cells in 2% glucose
100′ 104′ 108′ 112′ 116′ 120′ 124′ 128′ 132′ 136′ 140′ 144′ 148′ 152′
2.3
0.7
B
172′ 176′ 180′ 184′ 188′ 192′ 196′ 200′ 204′ 208′ 212′
336′ 340′ 344′ 348′ 352′ 356′ 360′ 364′ 368′ 372′ 376′
3.0
0.5
C
D
mean [ATP] (mM)
Time (min)

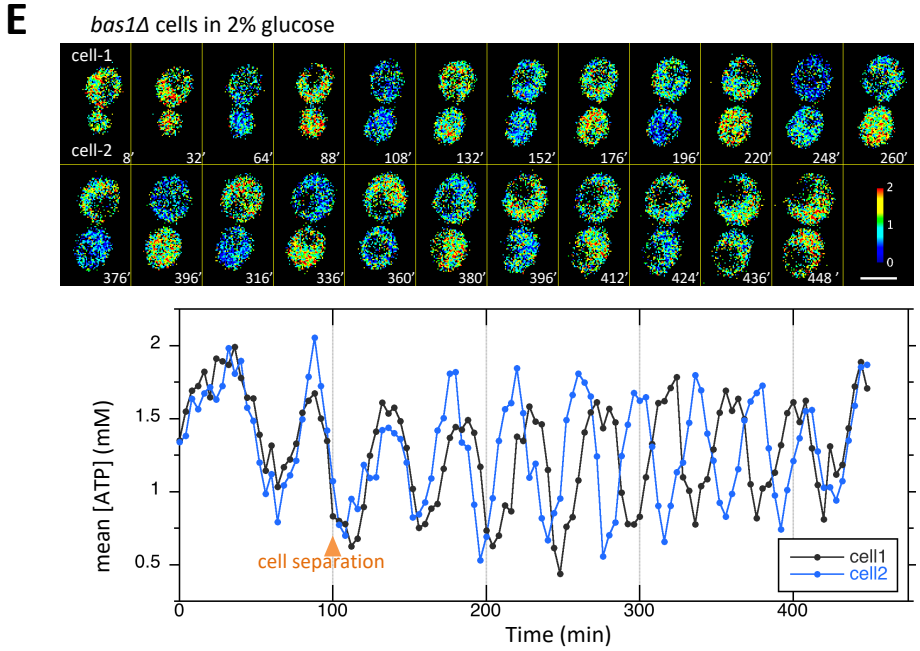
E
bas1Δ cells in 2% glucose
cell-1
cell-2
8′ 32′ 64′ 88′ 108′ 132′ 152′ 176′ 196′ 220′ 248′ 260′
376′ 396′ 316′ 336′ 360′ 380′ 396′ 412′ 424′ 436′ 448′
mean [ATP] (mM)
cell separation
cell1
cell2
Time (min)

Fig. 4

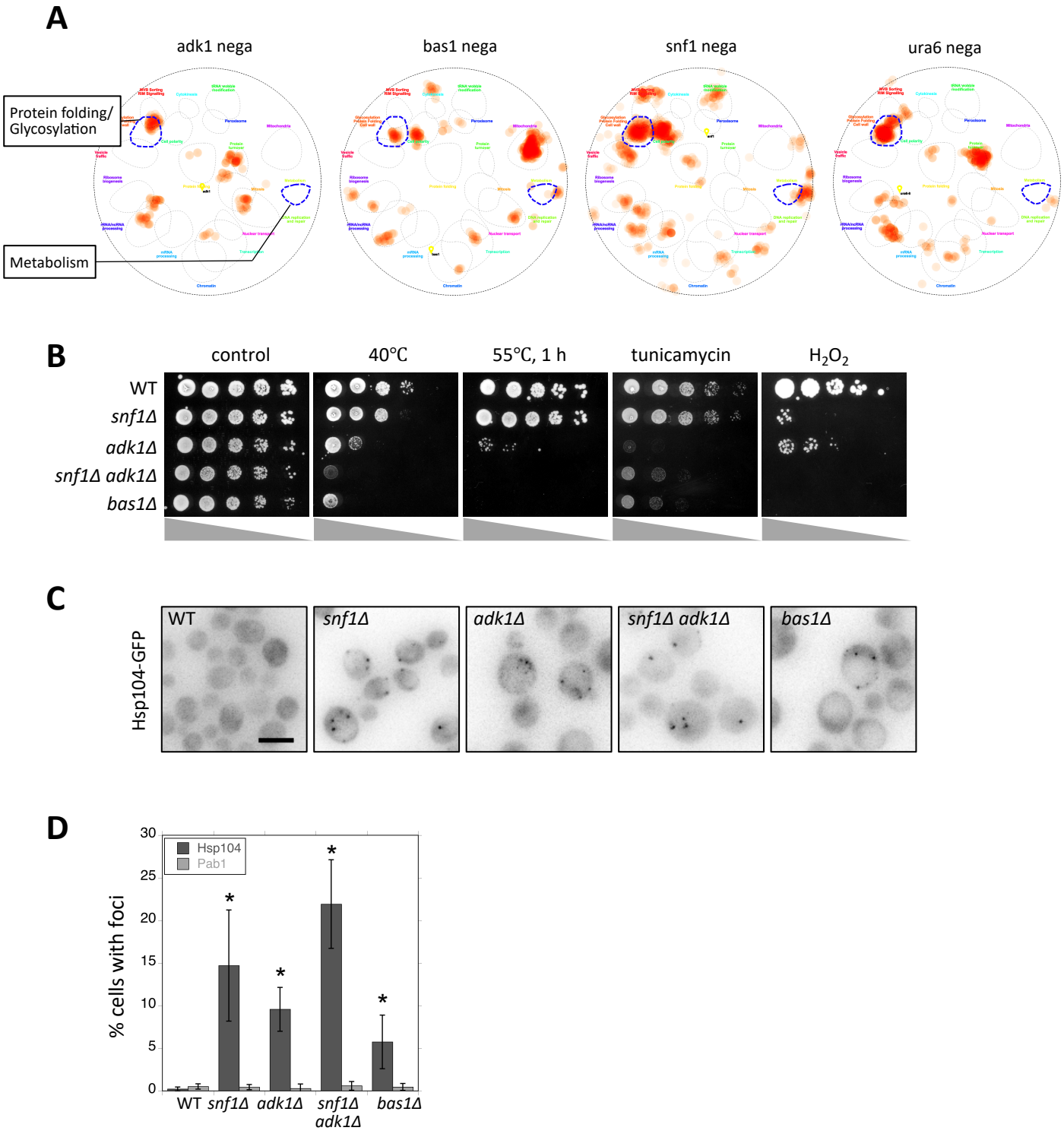
A
adk1 nega
bas1 nega
snf1 nega
ura6 nega
Protein folding/
Glycosylation
Metabolism
B
control
40°C
55°C, 1 h
tunicamycin
H2O2
WT
snf1Δ
adk1Δ
snf1Δ adk1Δ
bas1Δ
C
Hsp104-GFP
WT
snf1Δ
adk1Δ
snf1Δ adk1Δ
bas1Δ
D
% cells with foci
Hsp104
Pab1
WT
snf1Δ
adk1Δ
snf1Δ adk1Δ
bas1Δ

Fig. 5

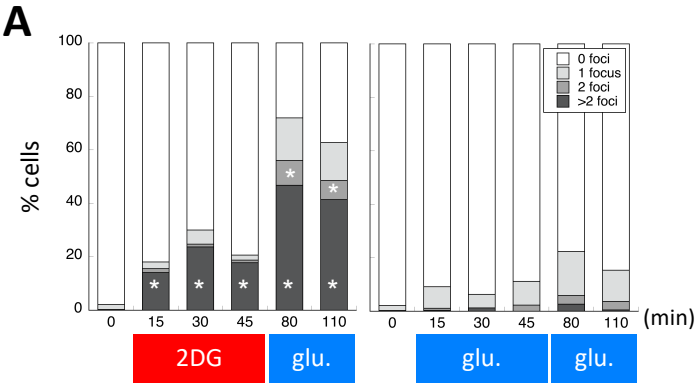
A
% cells
100
80
60
40
20
0
0 foci
1 focus
2 foci
>2 foci
0
15
30
45
80
110
(min)
2DG
glu.
glu.
glu.

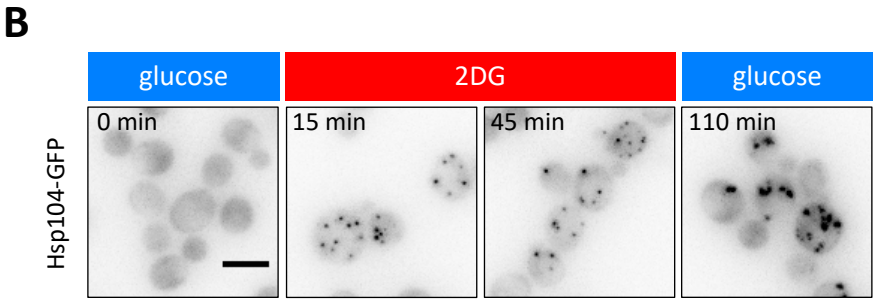
B
glucose
2DG
glucose
Hsp104-GFP
0 min
15 min
45 min
110 min

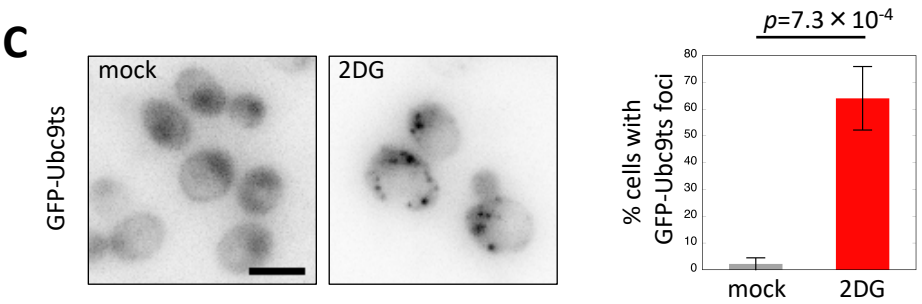
C
GFP-Ubc9ts
mock
2DG
p=7.3 × 10-4
% cells with GFP-Ubc9ts foci
80
70
60
50
40
30
20
10
0
mock
2DG

Fig. 6

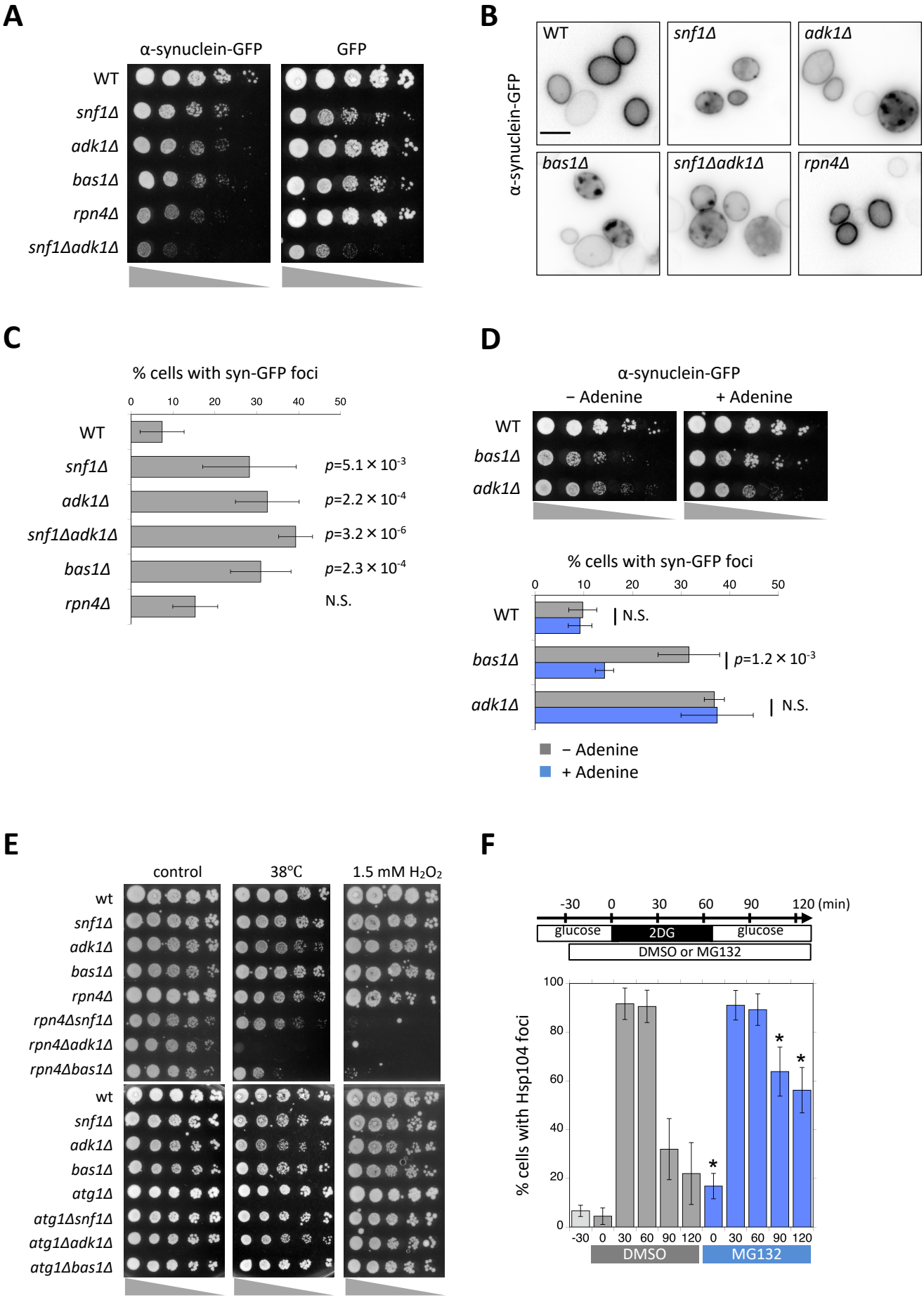
A
α-synuclein-GFP
GFP
WT
snf1Δ
adk1Δ
bas1Δ
rpn4Δ
snf1Δadk1Δ
B
α-synuclein-GFP
WT
snf1Δ
adk1Δ
bas1Δ
snf1Δadk1Δ
rpn4Δ
C
% cells with syn-GFP foci
0 10 20 30 40 50
WT
snf1Δ
adk1Δ
snf1Δadk1Δ
bas1Δ
rpn4Δ
p=5.1 × 10-3
p=2.2 × 10-4
p=3.2 × 10-6
p=2.3 × 10-4
N.S.
D
α-synuclein-GFP
− Adenine
+ Adenine
WT
bas1Δ
adk1Δ
% cells with syn-GFP foci
0 10 20 30 40 50
WT
N.S.
bas1Δ
p=1.2 × 10-3
adk1Δ
N.S.
− Adenine
+ Adenine
E
control
38°C
1.5 mM H2O2
wt
snf1Δ
adk1Δ
bas1Δ
rpn4Δ
rpn4Δsnf1Δ
rpn4Δadk1Δ
rpn4Δbas1Δ
wt
snf1Δ
adk1Δ
bas1Δ
atg1Δ
atg1Δsnf1Δ
atg1Δadk1Δ
atg1Δbas1Δ
F
-30 0 30 60 90 120 (min)
glucose
2DG
glucose
DMSO or MG132
% cells with Hsp104 foci
100
80
60
40
20
0
-30 0 30 60 90 120 0 30 60 90 120
DMSO
MG132

Fig. 7

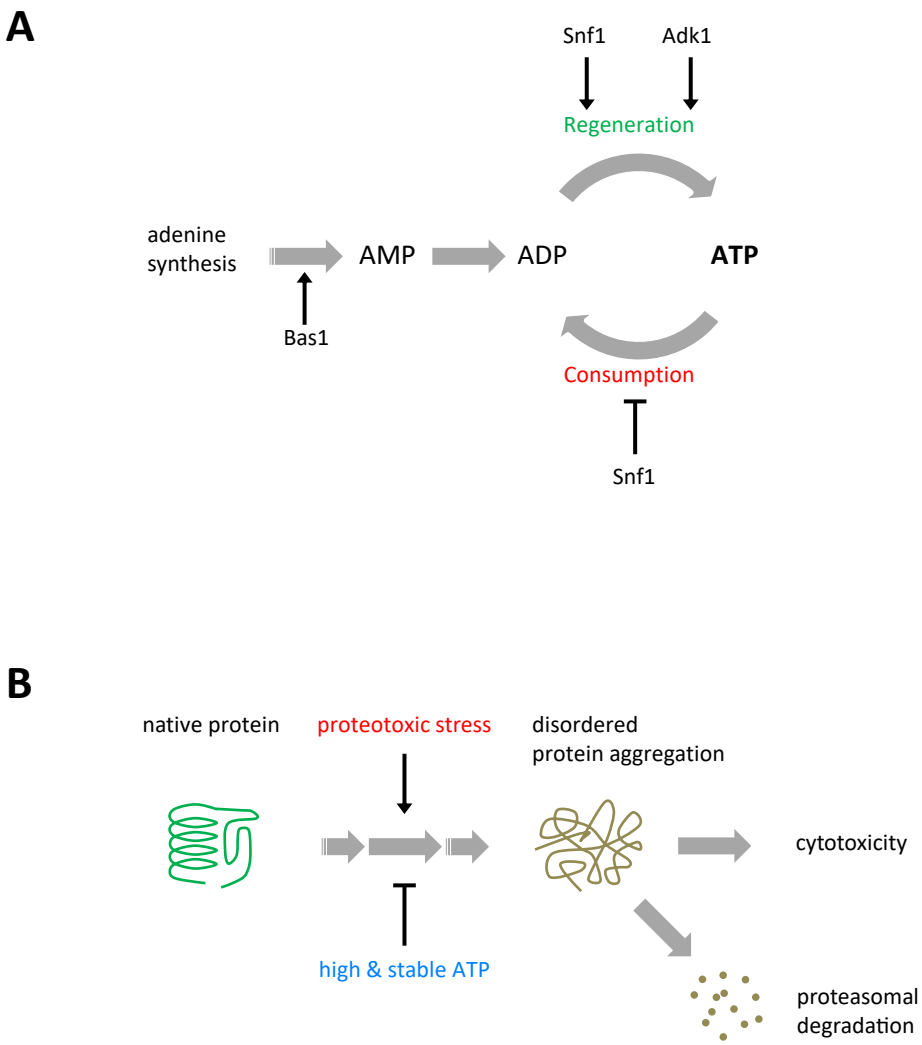
A
Snf1
Adk1
Regeneration
adenine
synthesis
AMP
ADP
ATP
Bas1
Consumption
Snf1
B
native protein
proteotoxic stress
disordered
protein aggregation
cytotoxicity
high & stable ATP
proteasomal
degradation

Fig. S1

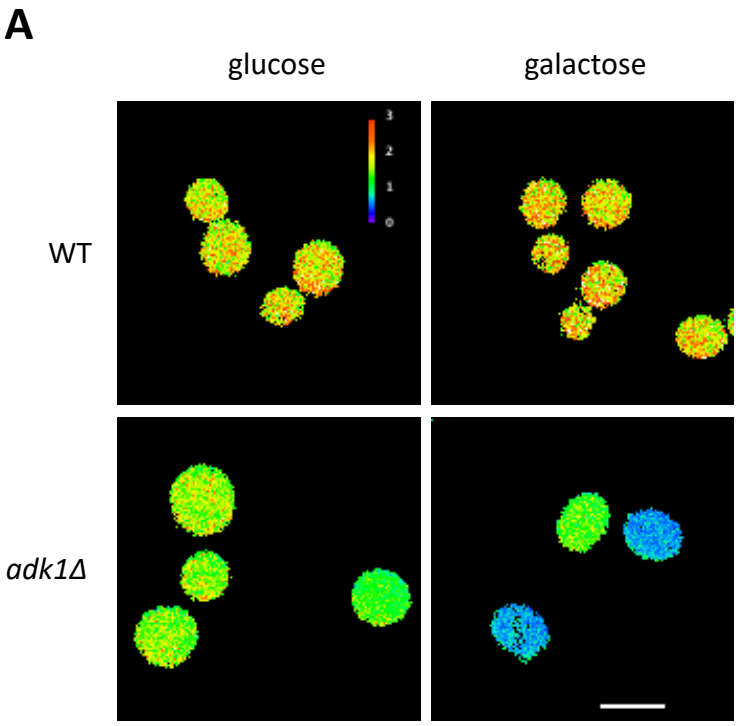
A
glucose
galactose
WT
adk1Δ
3
2
1
0

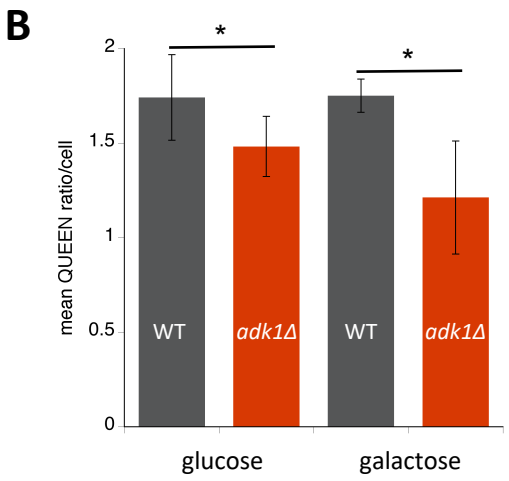
B
mean QUEEN ratio/cell
2
1.5
1
0.5
0
*
*
WT
adk1Δ
WT
adk1Δ
glucose
galactose

Fig. S2

A

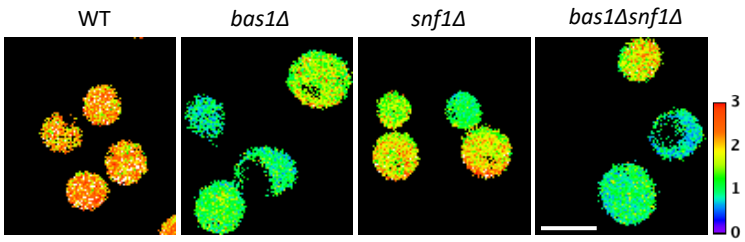

2% glucose

B

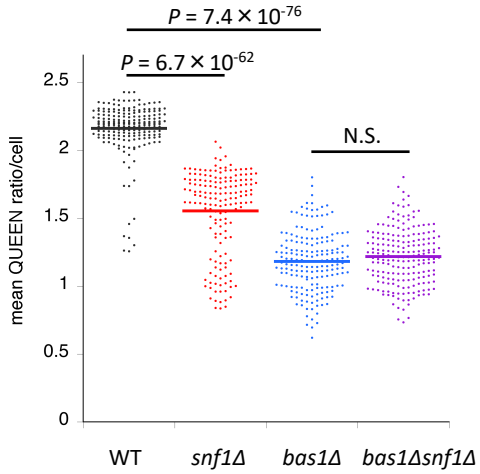

Fig. S3

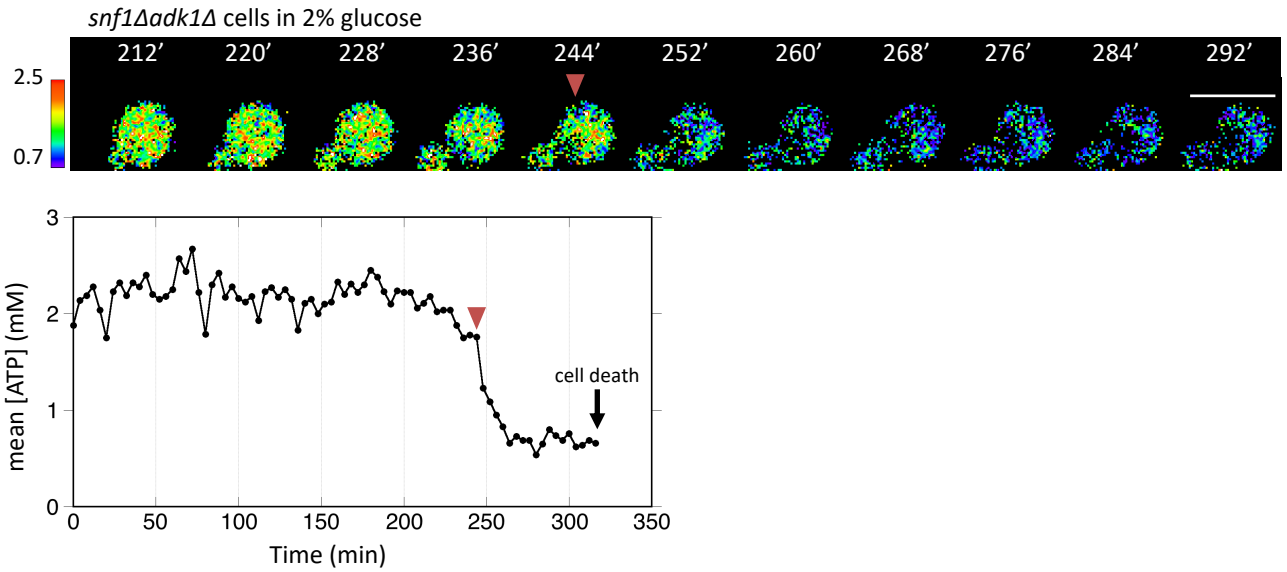
snf1Δadk1Δ cells in 2% glucose
212’
220’
228’
236’
244’
252’
260’
268’
276’
284’
292’
2.5
0.7
mean [ATP] (mM)
Time (min)
cell death
0
1
2
3
0
50
100
150
200
250
300
350

Fig. S4

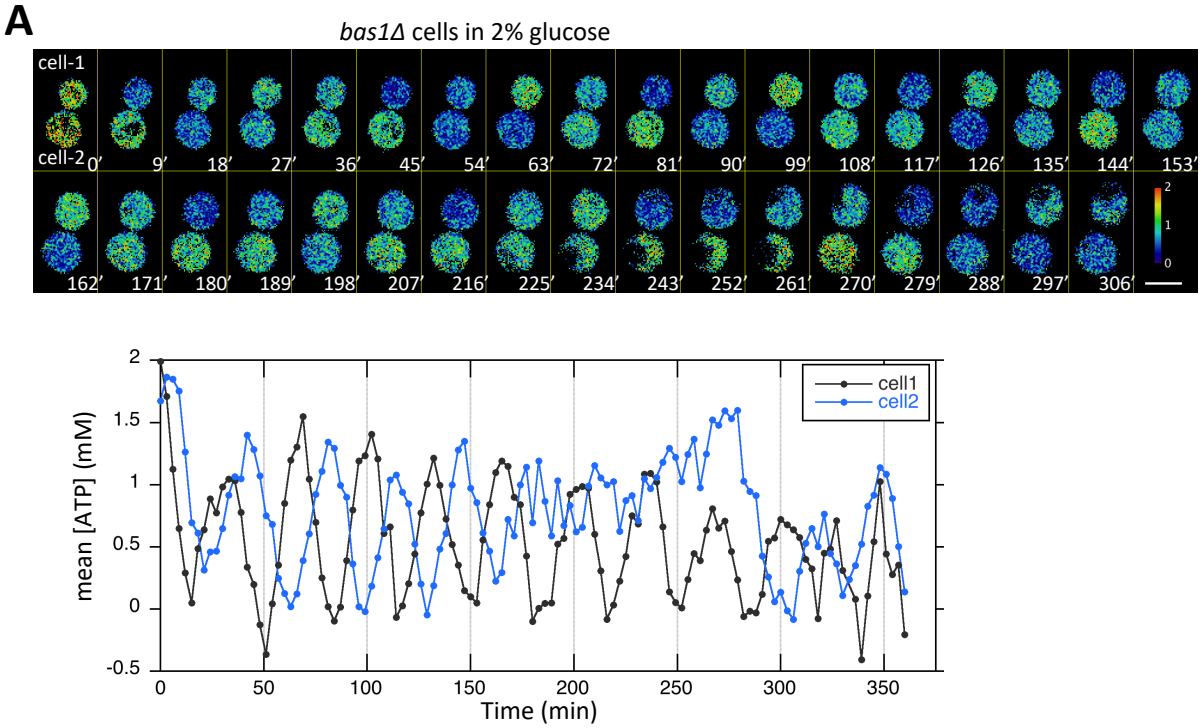
A
bas1Δ cells in 2% glucose
cell-1
cell-2
0′
9′
18′
27′
36′
45′
54′
63′
72′
81′
90′
99′
108′
117′
126′
135′
144′
153′
162′
171′
180′
189′
198′
207′
216′
225′
234′
243′
252′
261′
270′
279′
288′
297′
306′
2
1
0
mean [ATP] (mM)
Time (min)
cell1
cell2
B
correlation coefficient
Lag (frame)

Fig. S5

adk1 interactors

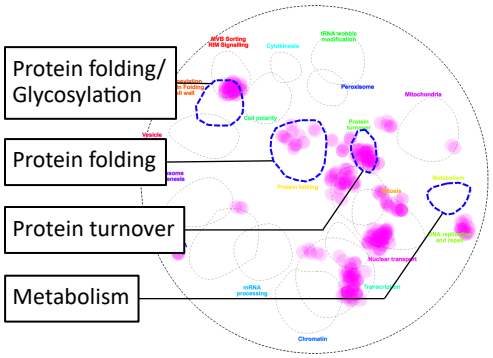

bas1 interactors

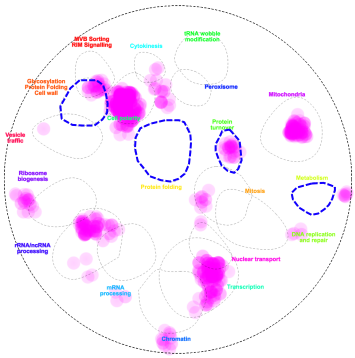

snf1 interactors

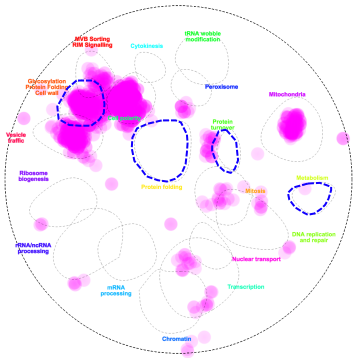

ura6 interactors

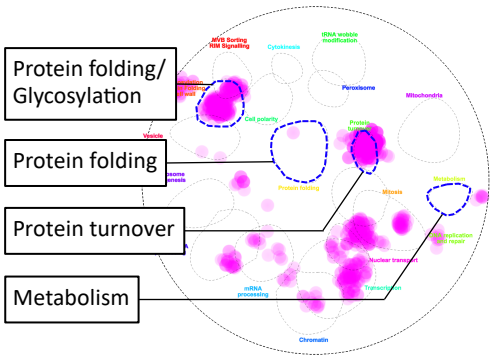

Fig. S6

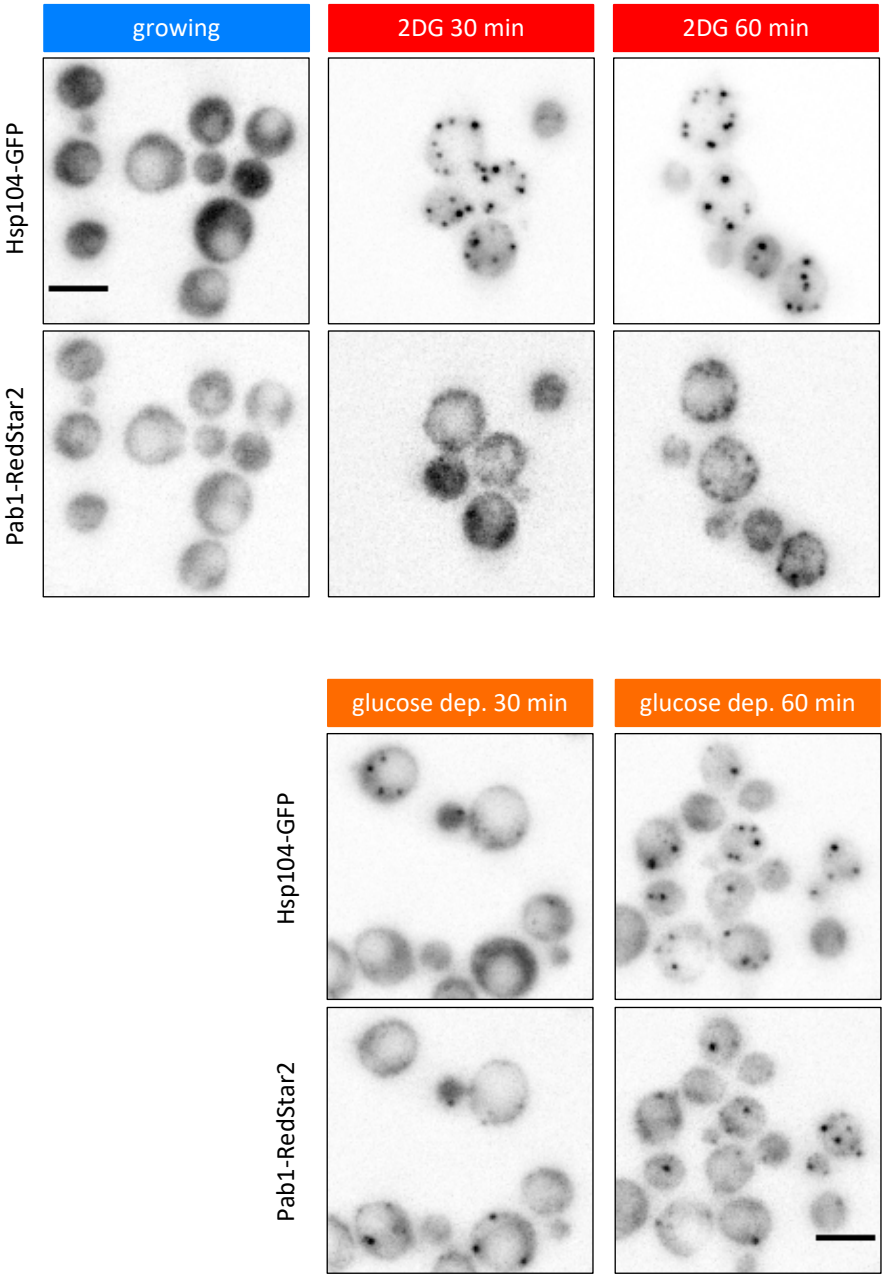
growing
2DG 30 min
2DG 60 min
Hsp104-GFP
Pab1-RedStar2
glucose dep. 30 min
glucose dep. 60 min
Hsp104-GFP
Pab1-RedStar2

Fig. S7